ISSN 1069-3513, Izvestiya, Physics of the Solid Earth, 2011, Vol. 47, No. 1, pp. 2–22. © Pleiades Publishing, Ltd., 2011.
Original Russian Text © A.A. Zhamaletdinov, A.N. Shevtsov, T.G. Korotkova, Yu.A. Kopytenko, V.S. Ismagilov, M.S. Petrishev, B.V. Efimov, M.B. Barannik, V.V. Kolobov, P.I. Prokopchuk, M.Yu. Smirnov, S.A. Vagin, M.I. Pertel, E.D. Tereshchenko, A.N. Vasil'ev, V.F. Grigoryev, M.B. Gokhberg, V.I. Trofimchik, Yu.M. Yampolsky, A.V. Koloskov, A.V. Fedorov, T. Korja, 2011, published in Fizika Zemli, 2011, No. 1, pp. 4–26.

Deep Electromagnetic Sounding of the Lithosphere in the Eastern Baltic (Fennoscandian) Shield with High-Power Controlled Sources and Industrial Power Transmission Lines (FENICS Experiment)

A. A. Zhamaletdinov[a,b,c], A. N. Shevtsov[a], T. G. Korotkova[a], Yu. A. Kopytenko[b], V. S. Ismagilov[b], M. S. Petrishev[b], B. V. Efimov [c], M. B. Barannik[c], V. V. Kolobov[c], P. I. Prokopchuk[c], M. Yu. Smirnov[d,j], S. A. Vagin[d], M. I. Pertel[d], E. D. Tereshchenko[e], A. N. Vasil'ev[e], V. F. Grigoryev[e], M. B. Gokhberg[f], V. I. Trofimchik[g], Yu. M. Yampolsky[h], A. V. Koloskov[h], A. V. Fedorov[i], and T. Korja[j]

[a] *Geological Institute, Kola Science Centre, Russian Academy of Sciences, ul. Fersmana 14, Apatity, 184209 Russia (GI KSC RAS)*

[b] *St. Petersburg Branch, Pushkov Institute of Terrestrial Magnetism, Ionosphere and Radio Wave Propagation, Russian Academy of Sciences, Muchnoi per. 2, St. Petersburg, 191023 Russia (SPbBIZMIRAN)*

[c] *Center for Physical and Technological Problems of Energy in Northern Areas, Kola Science Centre, Russian Academy of Sciences, ul. Fersmana 14, Apatity, Murmansk oblast, 184209 Russia (CPTPE NA KSC RAS)*

[d] *St. Petersburg State University, Universitetskaya nab. 7–9, St. Petersburg, 199034 Russia (SPbSU)*

[e] *Polar Geophysical Institute, Kola Science Centre, Russian Academy of Sciences, ul. Fersmana 14, Apatity, Murmansk oblast, 184209 Russia (PGI KSC RAS)*

[f] *Schmidt Institute of Physics of the Earth, Russian Academy of Sciences, ul. Bol'shaya Gruzinskaya 10, Moscow, 123995 Russia (IPE RAS)*

[g] *Russian North–West Bulk Power Systems, Kola, Murmansk oblast, Russia (RNW BPS)*

[h] *Institute of Radio Astronomy, National Academy of Sciences of the Ukraine, Kharkiv, Ukraine (IRA NASU)*

[i] *Kola Branch of Geophysical Survey, Russian Academy of Sciences, ul. Fersmana 14, Apatity, 184209 Russia (GS RAS)*

[j] *University of Oulu, Oulu, Finland (UOF)*

Received January 12, 2010

Abstract—The paper addresses the technique and the first results of a unique experiment on the deep tensor frequency electromagnetic sounding, the Fennoscandian Electrical conductivity from results of sounding with Natural and Controlled Sources (FENICS). In the experiment, Energy-1 and Energy-2 generators with power of up to 200 kW and two mutually orthogonal industrial 109- and 120-km-long power transmission lines were used. The sounding frequency range was 0.1–200 Hz. The signals were measured in the Kola–Karelian region, in Finland, on Svalbard, and in Ukraine at distances up to 2150 km from the source. The parameters of electric conductivity in the lithosphere are studied down to depths on the order of 50–70 km. A strong lateral homogeneity (the one-dimensionality) of a geoelectric section of the Earth's crust is revealed below depths of 10–15 km. At the same time, a region with reduced transverse crustal resistivity spread over about 80 000 square kilometers is identified within the depth interval from 20 to 40 km. On the southeast the contour of the anomaly borders the zone of deepening of the Moho boundary down to 60 km in Central Finland. The results are compared with the AMT–MT sounding data and a geodynamic interpretation of the obtained information is carried out.

Keywords: tensor frequency sounding, industrial power transmission lines, lithosphere, Baltic crystalline shield.

DOI: 10.1134/S1069351311010149

INTRODUCTION

The Baltic (Fennoscandian) crystalline shield is a convenient test site favorable for studying the depth structure and the thermodynamic state of the Earth's interior. Its huge area (over 1 mln km^2) and high degree of exposure facilitate these studies. The ancient Archaean and Proterozoic rocks are outcropping here. Large bodies of seismic, gravity, and magnetic surveys and electromagnetic soundings have been carried out on the territory of the Baltic shield. The state of the rock material has been studied under normal and high thermodynamic parameters. Based on the data available, a number of geological–geophysical models of the region have been developed [Zhamaletdinov, 1990; Glaznev, 2003]. Electromagnetic methods are the most challenging tool for deep studies in this region. Due to the absence of a conducting sedimen-

tary cover, the electromagnetic soundings on crystalline shields make it possible to obtain high-resolution indirect data on the material composition, fluid regimes, temperature, and the stress–strain state of the Earth's interior. Geophysicists paid attention to this fact as early as at the dawn of electromagnetic research [Kraev et al., 1947; Tikhonov et al., 1967]. However, investigations performed over a period of many years since that time, along with new discoveries, have posed a number of debatable questions concerning the nature and the structure of intermediate conducting layers in the crust, the parameters of a normal geoelectric section of the lithosphere, and many others. The solution of these problems necessitates the continuous improvement of the technique and methods for electromagnetic sounding with natural and controlled sources. Starting from 2005, the researchers of the Kola Scientific Center of the Russian Academy of Sciences in collaboration with the St. Petersburg Branch of the Pushkov Institute of the Earth's Magnetism, Ionosphere, and Distribution of Radio Waves (IZMIRAN) are working on the development of the technique of deep electromagnetic sounding using the industrial power transmission lines and Energy-1 and Energy-2 generators with power of 100 and 200 kW, respectively. This research is being conducted in the scope of the International FENICS experiment. The researchers from the Geological Institute and the Polar Geophysical Institute of the Kola Science Centre of the Russian Academy of Sciences (RAS), of the St. Petersburg Branch of IZMIRAN, the Geophysical Survey of RAS, the St. Petersburg State University, the University of Oulu (Finland), the Radio Astronomical Institute of the National Academy of Sciences of Ukraine (Kharkiv), and several other institutions were involved in experiments on the measurement of electromagnetic signals. The overall work on the design and construction of the Energy-1 and Energy-2 generators and generation of an electromagnetic field by the industrial power transmission lines (PTL) was carried out by the Center for Physical and Technological Problems of Energy in the Northern Areas, Kola Science Centre of RAS with the support of KolEnergo and Russia's North-West Bulk Power Systems.

The electromagnetic signals excited by the industrial PTL were measured both within the limits of the Baltic shield at distances up to 700 km from the source and beyond the shield, namely, on the Karelian isthmus ($r =$ 900 km), on Svalbard ($r =$ 1300 km), and in Ukraine ($r =$ 2150 km). The purpose of the remote measurements beyond the Baltic shield was to study the peculiarities in the electromagnetic signal propagation in the Earth–ionosphere waveguide, for problems of long-range low-frequency communication with submerged objects, prediction of earthquakes, etc.

In the present paper we will mainly focus on analyzing the measurements carried out within the Baltic crystalline shield with the aim to study the deep electrical conductivity and the thermal dynamic regime of the lithosphere and to develop the technique for the exploration and prospecting of mineral deposits.

THE TECHNIQUE OF THE FENICS EXPERIMENT

The key feature of the frequency electromagnetic sounding in the FENICS experiment is the application of two mutually orthogonal industrial power transmission lines connected to a high-power (up to 200 kW) generator of extremely low-frequency (ELF) and ultralow-frequency (ULF) signals in the frequency range of 0.1–200 Hz. With this setup it is possible to "illuminate" the deep structure of the lithosphere at two mutually orthogonal polarizations of the primary field (here and below the lithosphere is understood as a crystalline shell of the Earth, which includes the crust and the upper mantle). In its turn, this fact allows one to closely approach the technique of sounding with controlled sources to the traditional methods of audio magnetotelluric (AMT) and magnetotelluric (MT) sounding based on the use of natural sources of thunderstorm and magnetospheric–ionospheric origin. Note that in all the previous large-scale experiments on deep and superdeep sounding of the lithosphere with controlled sources known in the world practice, as a rule, the schemes with a single orientation of the power line were employed. The soundings themselves were conducted in a dc current mode [Kraev et al., 1947; Cantwell et al., 1965; Van Zijl, 1969; Blohm et al., 1977] or as the transient electromagnetic sounding at the fronts of rectangular current pulses [Sapuzhak and Enenshein, 1980; Zhamaletdinov et al., 1982]. The technique employing high-power ELF–ULF radiating systems and two mutually orthogonal industrial power transmission lines (PTL), described in the present paper, has no direct counterpart in foreign or Russian practice of deep electromagnetic sounding of the lithosphere.

Figure 1 shows the principle circuit of a tensor sounding with controlled sources. We named this technique the controlled source magnetotellurics (CSMT) [Zamaletdinov et al., 2007]. Compared to the well-known method of controlled–source audio magnetotelluric sounding in the audio frequency range (CSAMT) [Boerner, 1991; Zonge and Hughes, 1991], the CSMT sounding technique is intended for operation in the range of extremely low and ultralow frequencies (ELF–ULF) at the boundary frequencies between MT and AMT methods (0.1–200 Hz) and is applied for studying the electrical conductivity of the lithosphere at depths from a few to 50–70 km. However, such a large penetration depth of the field in the given frequency range can be attained only at the segments of the earth's surface with a high electrical resistivity ($\rho \geq 10^4\ \Omega$ m), that is, only within the crystalline shields. The depth of the sounding with the plane wave excitation can be estimated according to the formula $h_S = \frac{1}{2\pi}\sqrt{\frac{10^7\rho}{2f}}$ m [Zhdanov et al., 1986]. It can be easily seen that the maximum depth of ELF sounding (0.1 Hz and higher) in the platform regions where the

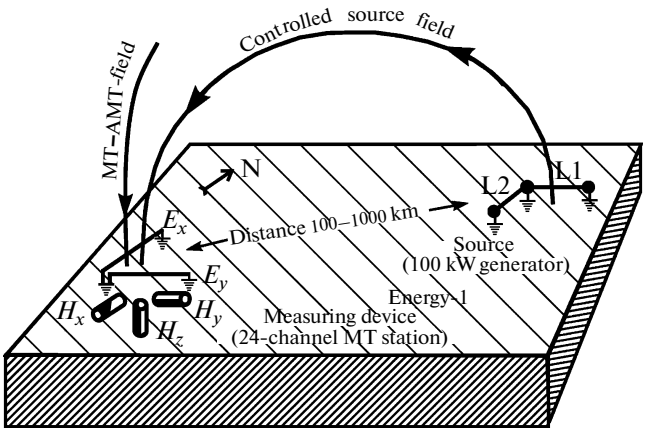

Fig. 1. Schematic setup of tensor frequency electromagnetic sounding in the field of two mutually orthogonal transmission lines (industrial PTLs) in the ELF–ULF range (Controlled Source Magnetotellurics, CSMT).

resistivity of the sedimentary cover is, on average, 10 Ω m, will be a few kilometers as shallow.

The signal recording in the CSMT method is conducted using broad-band five-component 24-channel digital stations (Fig. 1). Natural variations in the Earth's magnetic field and the signals from a controlled source are simultaneously recorded by one and the same MT–AMT stations. The harmonic signals from a controlled source are distinguished against the background variations in the MT–AMT field using the fast Fourier transform procedure (FFT) or any other methods of digital filtering. Application of two mutually orthogonal power transmission lines (polarizations) makes it possible to estimate the dimensionality of the lower half-space at the stage of data interpretation and to take into account the possible effects of a horizontal two- or three-dimensional inhomogeneity of the geoelectric medium in the same way as it is done in the MTS method. With this aim, special additional approaches to the analysis of the primary data can be applied, which allow for the properties of the normal field generated by the controlled source. The present paper will mainly focus on the technique and the results of the measurements with a controlled source. A comparison with the results of the MT–AMT sounding will be made as the material is considered.

TRANSMITTING UNIT SCHEMATIC

A schematic configuration of the sounding setup using industrial PTLs is presented in Fig. 2 that exemplifies the connection of the Energy-2 generator to the 120 km-long Kola-Monchegorsk PTL. The Energy-2 ELF–ULF generator can be powered by any three-phase transformer with output voltage of 380 V to supply the required consumed power of 100–200 kW (a stationary auxiliary transformer of an electric power substation or a mobile diesel generator). The voltage of the three-phase transformer is fed to a set-up converter (SUC). A dc voltage of 1100 V is generated at the SUC output. This voltage is supplied to a high-voltage inverter (HI), which generates a sine current of a given frequency in the antenna load (this is done using the pulse-width modulation (PWM) method). Depending on the problem to be solved, the shape of the current can be arbitrary, e.g., a sine, a meander, a triangle. The maximal amplitude voltage at the HI output attains 1100 V.

In the Energy-2 generator the possibility is also provided for feeding from two dc self-generators (DCG-1 and DCG-2 in Fig. 2) of a ZIL-131 auto truck in which all the main units of the Energy-2 generator are arranged. The dc generators with the output voltage of 500 V are connected in series in order to produce an output dc voltage of 1000 V. This voltage is supplied directly to the high-voltage inverter (HI). In the off-line mode of operation, the power in the load is determined by the maximal output power of the DCG (30 kW).

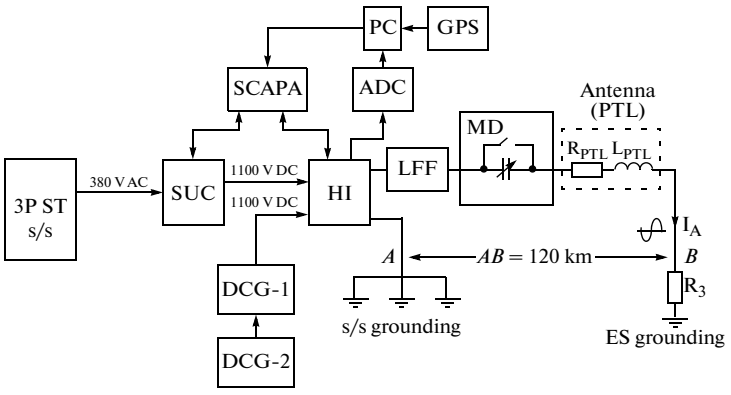

Fig. 2. Generalized structural circuit of the ELF–ULF Energy-2 generator. (3P ST S/S) a three-phase supply transformer of a substation; (DCG-1, DCG-2) dc generators of ZIL-131 truck with the Energy-2 generator mounted in its wagon; (SUC) set-up converter; (HI) high-voltage inverter; (LFF) low frequency filter; (MD) matching device (a battery of compensating capacities); (SCAPA) system of controlling, adjustment, protection and automation; (ADC) analog-to-digital converter; (PC) personal computer; (GPS)time synchronization GLONAS/GPS module.

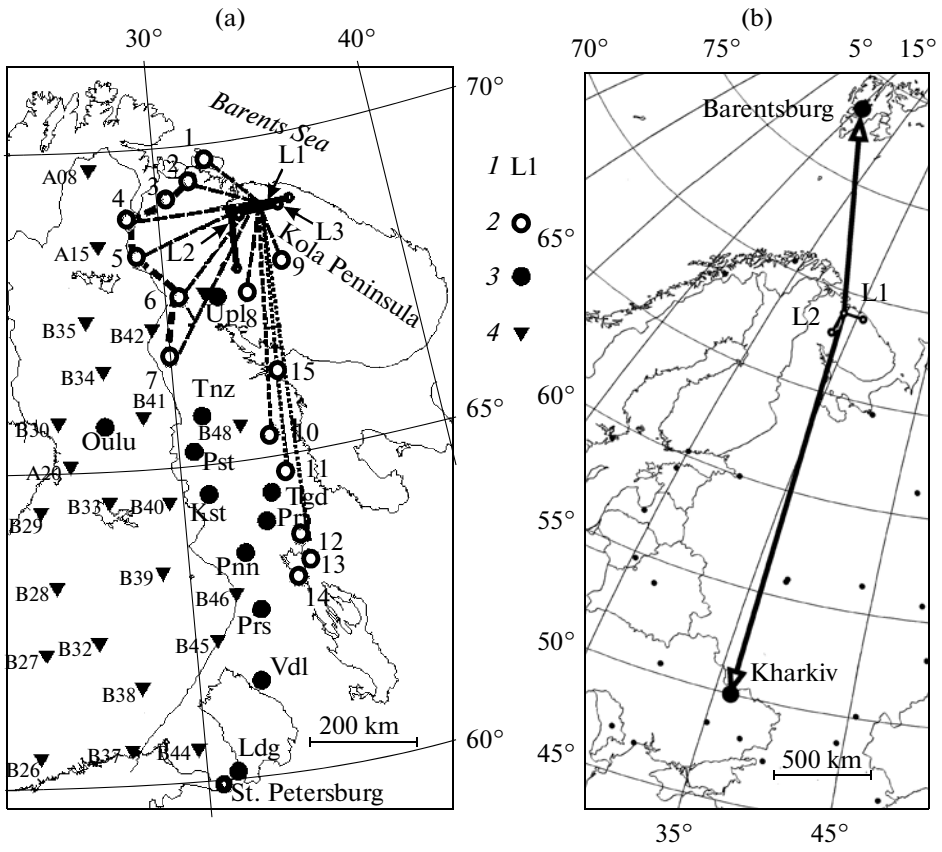

Fig. 3. Locations of the transmission and the receiving lines in the FENICS experiment: (a) the locations of the nearest receiving points within the eastern part of the Baltic shield; (b) locations of the remote receiving points. Legend for Fig. 3a: (*1*) supply lines L1, L2, and L3; (*2*) sounding stations in the FENICS-2009 experiment; (*3*) sounding stations in the FENICS-2007 experiment; (*4*) MTS stations in the BEAR–1998 experiment [Korja et al., 2002]. The geographical names of the sounding stations in the FENICS-2007 and FENICS-2009 experiments are explained in Table 1 and in the text.

The main functional units of the Energy-2 generator (BC and HI in Fig. 2) are described in [Tereshenko et al., 2008; Barannik et al., 2009] and are not considered here.

The arrangement of the power lines in the FENICS experiment is shown in Fig. 3. The near-latitudinal L1 Kola–Serebryanka power transmission line is 109 km long. The L2 Kola–Monchegorsk power transmission line is directed north–south and is 120 km long. Besides the L1 and L2 lines, also the 55-km long L3 power transmission line, namely, one of the antennas of the Zevs ELF transmitter was used at times [Velikhov et al., 1994]. The first harmonics current in L1 varied from 170–235 A at low frequencies (0.1–10 Hz) to 25–60 A at high frequencies (100–200 Hz). The resistance of L2 is twice as high as that of L1 and, thus, the current in the L2 line followed another pattern, varying from 100–120 A at low frequencies (0.1–10 Hz) to 40–80 A at high frequencies (100–200 A). At frequencies in excess of 5–10 Hz, the reactance of PTL was compensated using an impedance matching device (MD in Fig. 2). The sine current in the transmitting antennas was recorded in a PC via E-140 ADC with a sampling frequency of 5 kHz. The frequency stability was 10^{-7} Hz. The current in the transmitting antennas and the signals at the receiver stations were synchronized via a global satellite positioning GPS system, with an accuracy not less than 10^{-2} s.

THE ANALYSIS OF THE RESULTS OF PRELIMINARY DATA PROCESSING

The FENICS measurements were conducted in the Kola–Karel region in Northwest Russia, North Finland, on Svalbard, and in Ukraine. The locations of the power lines and the sounding stations are shown in Fig. 3a for the nearest sounding sites arranged within the eastern part of the Baltic shield and its borders. A similar map for the farthest stations in the Barentsburg observatory (on Svalbard) and near Kharkiv (Ukraine) is presented in Fig. 3b. The transcript of the geographical names of the sounding sites in Fig. 3a is given below in Table 1. Also, the organizations involved in the measurements are listed in the Table 1.

The time series of the measurement data are stored in a uniform database of raw FENICS data. The program is developed for spectral processing of the measured signals synchronously with the records of current in the transmit-

Table 1. Sounding stations

Station symbol	Geographical name	Organization	Station mark	Geographical name	Organization
Upl	Upoloksha	GI KSC RAS	3	Shuoni-Pechenga	GI KSC RAS
Tnz	Tungozero	″	4	Rayakoski	″
Pst	Pisto	″	5	Svetloe	″
Kst	Kostomuksha	″	6	Kovdor	″
Pnn	Peninga	″	7	Alakurtti	″
Prs	Porosozero	″	8	Apatity	GS RAS
Tgd	Tunguda	″	9	Lovozero	PGI KSC RAS
Prt	Pertozero	NIIP SPbSU	10	Kuzema	SPbBIZMIRAN
Vdl	Vidlitsa	SPbBIZMIRAN	11	Lekhta	″
Ldg	Ladoga	IEC SPbSU	12	Segezha	″
Oulu	Oulu	Oulu Univ., Finl.	13	Popov Porog	″
1	Rybachii	GI KSC RAS	14	Segozero	″
2	Karik–Yavr	″	15	Belyi Isl.	NIIP SPbSU

ting antennas. Figure 4 displays an example of spectral processing of the electric and magnetic field components in the FENICS-2007 experiment.

The results of data preprocessing are represented in terms of spectral power density (SPD). All the measurements presented in Fig. 4 were carried out in the field of the near-latitudinal power transmission line L1. The corresponding SPD curve of the current intensity in L1 is plotted in the bottom left corner in Fig. 4. The analysis of SPD diagrams in Fig. 4 gives a general idea about the type of the deep geoelectric section. A pronounced increase in the intensity of electric and magnetic field components in the middle frequency range of 2–20 Hz points to the fact that the resistivity of the middle part of the lithosphere increases with depth and then decreases, i.e., the depth section belongs to the K– type ($\rho_1 < \rho_2 > \rho_3$). In all the graphs of natural noise, the first harmonic of the Schuman resonance at 8 Hz and its higher harmonics are clearly apparent.

The results of signal recording in the FENICS-2009 experiment at a distance of 2150 km are presented in Fig. 5. The signals were recorded at the low-frequency observatory (LFO) of the Institute of Radio Astronomy with the National Academy of Sciences of Ukraine (Martovoe village, Kharkiv region, 49°56′N, 36°57′E). The signals were measured using two devices, namely, the Lemi–017 fluxgate magnetometer (0–0.5 Hz) and the ULF complex with induction sensors (0.5–40 Hz) [Paznukhov et al., 2010]. The time of signal accumulation in the spectral analysis was $T = 500$ s (with 0.002 Hz frequency resolution). The selected interval of analysis allowed us to reach an exact frequency match in the reconstructed spectra of ELF–ULF signals generated by the Energy-2 generator. The signals from the near-latitudinal power transmission line L1 were recorded at frequencies of 0.642, 0.942, 1.422, 3.822, 6.422, 9.422, 19.42, and 38.22 Hz. A typical amplitude spectrum of the signal at a frequency of 0.642 Hz is shown in Fig. 5. The signal is most pronounced in the meridional component B_x (orthogonal to the power line) and is substantially weaker in the B_y component (parallel to the power line), which is in full agreement with the directional pattern of the primary field. We failed to detect the signals from the L2 submeridional transmitting antenna. It means that the receiving point was located within the quasi-stationary wave zone where the bias effect is insufficient to entail a rotation of the directional pattern by 90°, according to the calculations reported in [Bernstein et al., 1974; Akindinov et al., 1976].

The measured signals were recalculated into the apparent resistivity values using two types of normalization, namely, by the input impedance and by the electric field. By analogy with the technique of MT data processing [Berdichevsky, 1968], in case of normalization based on the input impedance, it is sufficient to know the exact amplitude of the electric and magnetic fields and the generator frequency:

$$\rho_{\mathrm{T}}^{xy}(f) = 0.127\mathrm{T}\left|\frac{E_x(f)}{H_y(f)}\right|^2, \quad \rho_{\mathrm{T}}^{yx}(f) = 0.127\mathrm{T}\left|\frac{E_y(f)}{H_x(f)}\right|^2,$$

$$\varphi_Z^{xy} = \varphi_{E_x} - \varphi_{H_y}, \quad \varphi_Z^{yx} = \varphi_{E_y} - \varphi_{H_x},$$

where T is the period of the signal in seconds; $E_x(f)$ and $E_y(f)$ is the intensity of the electric field in the north–south and east–west directions measured in V/m at a frequency f, respectively; $H_x(f)$ and $H_y(f)$ is the magnetic field intensity in mA/m in the same directions.

Normalization based on the electric component in the wave zone [Vanyan, 1965] requires that both the field intensity at the signal receiving point and the parameters of the receiving and the feed units are known, including the generator current in the transmitting antenna. The apparent resistivity is calculated in this case using the equations

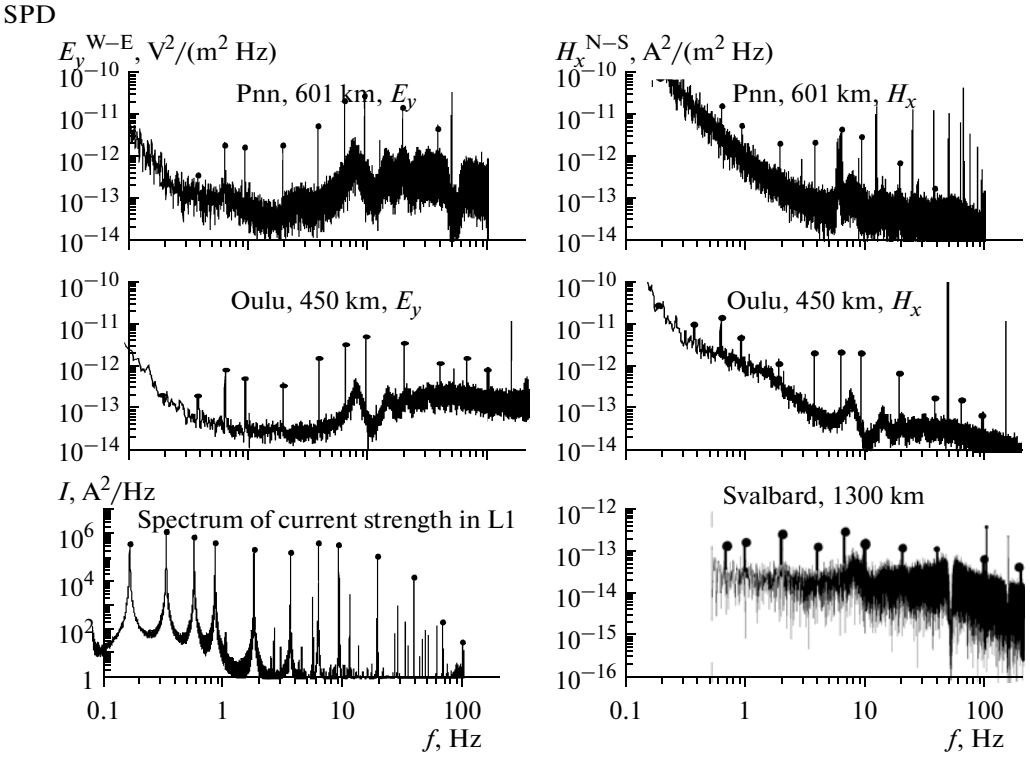

Fig. 4. Diagrams of spectral power density (SPD) according to the data of FENICS-2007 experiment. Electric (E_y, EW) and magnetic (H_x, NS) components were measured in the field of the sublatitudinal power transmission line L1 at different distances from it: (1) 450 km, Northern Finland, Oulu University, MTU2000 station, (2) 601 km, Southern Karelia, Peninga, GI KSC RAS, SChZ-station, and (3) 1300 km, Svalbard, Barentsburg, the station of PGI KSC RAS). SPD-1 is the spectrum of the first-harmonic current intensity in L1. The position of the supply line L1 and locations of the receiving points are shown in Fig. 2.

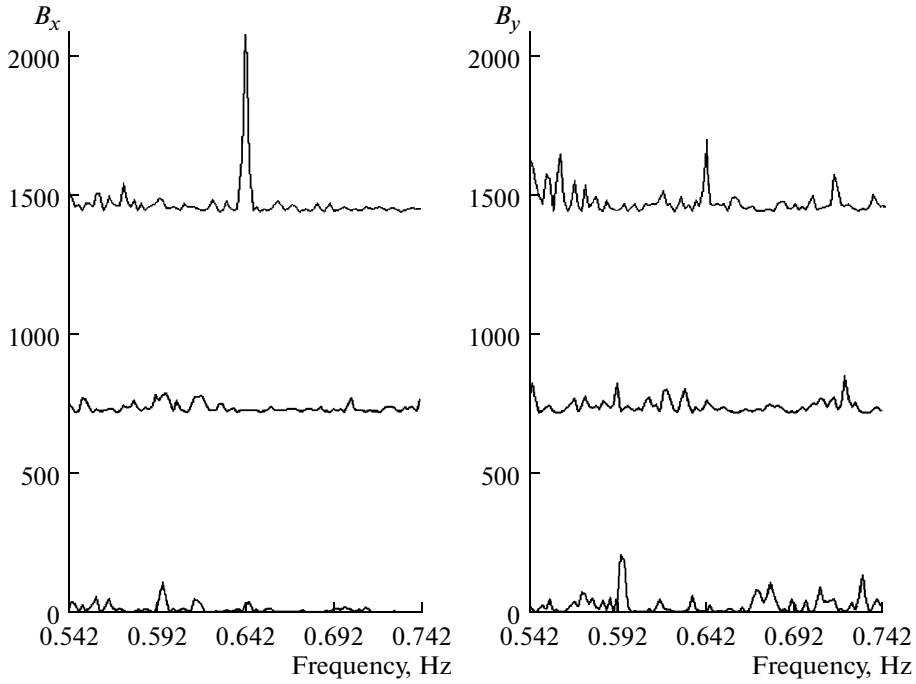

Fig. 5. The spectra of the signals transmitted by the sublatitudinal line L1 measured near Kharkiv at a distance of 2150 km from the source at the frequency of 0.642 Hz, according to on the data of FENICS-2009 experiment (Station Lemi-7 and an ULF-complex. The LF observatory of the Institute of Radio Astronomy of the National Academy of Sciences of the Ukraine).

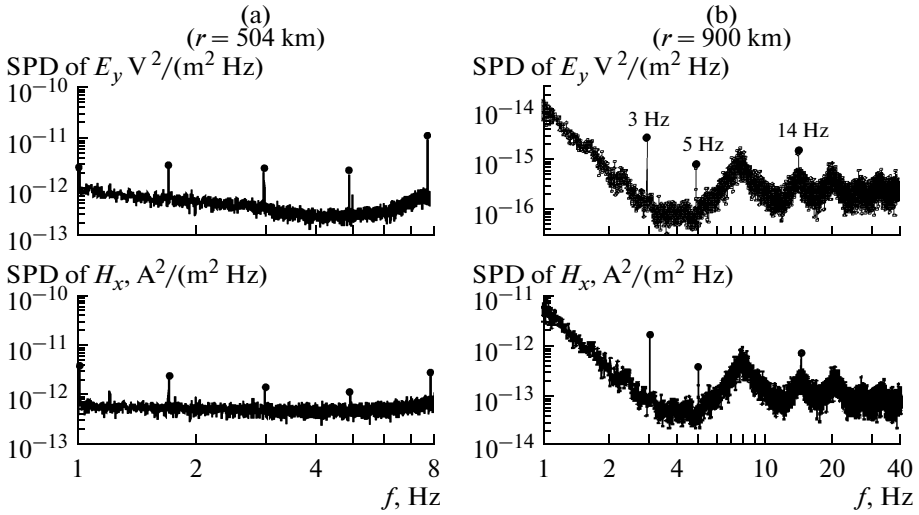

Fig. 6. Diagrams of spectral power density (SPD) of the electric and magnetic field components, according to the results of processing of the signals generated (a) by the L1 line in Lekhta at a distance of 504 km and (b) by the L3 line in Ladoga at a distance of 900 km. The locations of the supply lines L1 and L3 and the locations of the measurement stations are shown in Fig. 3a (Lekhta is marked by 11 and Ladoga is abbreviated as Ldg).

$$\rho_a^{E_x}(f) = K\frac{E_x(f)}{I(f)} \text{ and } \rho_a^{Ey}(f) = K\frac{E_y(f)}{I(f)},$$

where $E_x(f)$ and $E_y(f)$ is the electric field intensity in V/m measured at the frequency f in the north–south and east–west directions, respectively; $I(f)$ is the current of the first harmonic in amperes; and K is the geometry factor of the setup taking into account the mutual location and the dimensions of the power supply and receiving lines. In the dipole approximation, the geometry factor K for the quasi-stationary far-field (wave) zone has the form

$$K = \frac{2\pi r^3}{AB(3\cos^2\theta - 2)},$$

where AB is the length of the grounded transmitting power line in meters, r is the distance between the transmitter and the receiver in meters, and θ is the angle between the power line AB connecting the ends of the grounded supply line (PTL) and the direction from the middle of AB to the receiving point. Under the conditions of the FENICS experiment where the lengths of the supply lines were of the same order as the spacing, the geometry factor K was calculated at each point for the real configuration of the PTL feeding cable taking into account the nondipole setup pattern [Shevtsov, 2006].

Figure 6 illustrates the results of spectral processing of the data obtained at the Lekhta station (11 in Fig. 3, r = 504 km) and Ladoga (Ldg in Fig. 3, r = 900 km) by the example of the latitudinal electric (E_y) and the meridional magnetic (H_x) field components. The measurements at Lekhta were conducted for the 109 km-long near-latitudinal industrial power transmission line L1 using the GI MTS-1 station with torsion magnetometers (St. Petersburg Branch of IZMIRAN). The measurements at the Ladoga station were carried out using the AKF-4 station with induction sensors (Earth Crust Institute of SPbSU) for the radiation from the sublatitudinal power transmission line L3 (the Zevs ULF antenna fed by the Energy-1 generator). It is apparent that the SPD amplitude of the magnetic field at the Ladoga station is about 1.5 times smaller, and that of the electric field is 3 times smaller their counterparts at the Lekhta site. This is first of all due to the Ladoga site being twice as remote and to the fact that the 55-km long L3 antenna is twice as short as the L1 antenna. In addition, the resistance of cables and grounding of L3 is two times higher. Therefore, the current in this line was almost half the current in L1. Nevertheless, despite such a large difference in the radiation amplitudes at the Ladoga and Lekhta stations, the signal-to-noise ratio in the magnetic field records in Fig. 6 is nearly the same, ranging from 5 to 20 dB, which confirms the evident advantage of the induction sensors over the torsion ones for recording ELF-ULF signals.

It should be also noted that the Ladoga station is located in the region composed of highly conductive pre-Cambrian shales at the outer surroundings of the Baltic shield, which results, among other, in low amplitudes of the electric field component. For example, at a frequency of 5 Hz, the SPD is 10^{-15} V^2/(m^2 Hz). The frequency step is Δf = 0.005 Hz. Using the relation $E = \sqrt{\text{SPD}\Delta f}$, one can readily estimate the electric field as $E_y = 2.3 \times 10^{-3}$ mV/km. The length of the receiving line is 100 m and, thus, the measured voltage ΔU at the input of the station was negligibly small, namely, 2.3×10^{-7} V (230 nV). The noise amplitude of the natural field at the same frequency is about 10^{-3} mV/km (100 nV for a 100-m-long power transmission line). The SPD

of the intrinsic instrumental noise at a frequency of 5 Hz is estimated to be 1.6×10^{-15} V^2/(m^2 Hz). The frequency step in both cases is the same (0.005 Hz). Thus, the voltage of the internal noise at a frequency of 5 Hz is about 2.8 nV, which is nearly two orders of magnitude lower than the measured voltage of 230 nV. These estimates demonstrate the large potentialities of modern digital stations in recording weak signals from controlled sources against noise.

The apparent resistivity and the impedance phase yielded by processing the AMT–MT and CSMT sounding data at the Ladoga site are shown in Fig. 7. The apparent resistivity in AMT–MT sounding curves grows with the increasing period of T, which indicates the presence of the shallow poorly-conducting crystalline basement. The ascending branch of ρ_T is tilted at 45° to the axis of periods T, which corresponds to an inclination of 63° in the coordinates (ρ_T, $\sqrt{T}$). Based on this reasoning, one can estimate the longitudinal conductivity S of the sedimentary cover in accordance with the asymptotic expression $S = 356\sqrt{T/\rho}$, where T, ρ are the coordinates of any point on the ascending asymptotic branch of the apparent resistivity [Berdichevsky, 1968]. An approximate estimate of S is 25 S. Judging from the left high-frequency branch, the average resistivity of the upper sedimentary formations is 10–20 Ω m and, thus, the depth to the basement ranges from 0.25 to 0.5 km.

In Fig. 7 we also see a good agreement between the values of apparent resistivity and phase impedance yielded by the AMT–MT sounding in the natural field variations and the results of CSMT in the field generated by a controlled source. This suggests that the deep sounding with a controlled source presents no advantage over the AMT–MT sounding and, thus, it is not necessary to apply a complex CSMT technique that requires bulky and expensive generator devices. However, this conclusion is more or less valid only for sounding on the surface of highly conductive rock where the penetration depth of the electromagnetic field is small. In these conditions, the effect of the lateral inhomogeneity of the medium is also weak, and the influence of industrial noises and lightning discharges on the initial structure of the AMT field is negligible. Without going deeper into this subject, which requires special consideration, let us turn back to the topic discussed in the present paper, namely, to the study of the deep electric conductivity of the Baltic shield.

An important advantage of CSMT sounding is the possibility for the joint analysis of the processed data using the impedance and the geometrical (component) approaches. In combination with AMT–MT sounding, it expands the range of informative parameters. An example of such analysis is presented in Fig. 8.

Figure 8 displays the results of measurements at the Peninga (Pnn) ($r = 603$ km) and Porosozero (Prs) ($r = 701$ km) sites. The measurements were performed using the SChZ–2002 station of the Geological Institute

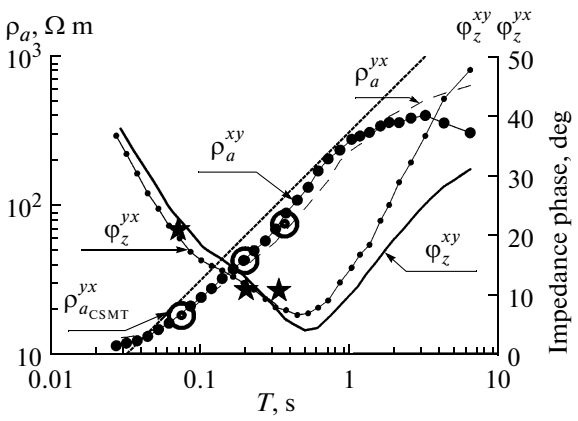

Fig. 7. Apparent resistivity and impedance phase curves calculated from the data of CSMT and AMT–MT sounding at Ladoga station 900 km away from the sublatitudinal power line L3. The locations of L3 line and Ladoga station (Ldg) are shown in Fig. 3a. The symbols on the curves are: ρ_a^{xy} and ρ_a^{yx} are the curves of apparent resistivity in the field of natural MT–AMT variations; φ_z^{xy}, and φ_z^{yx} are the impedance phases; $\rho_{a\mathrm{CSMT}}^{yx}$ (circles with dots) are the apparent resistivities calculated from the data of CSMT measurements in the field generated by L3 line at 3, 5, and 14 Hz; $\varphi_{z\mathrm{CSMT}}^{yx}$ (asterisks) are the impedance phases.

of the Kola Science Centre RAS in the field of the L1 near-latitudinal power transmission line.

The same data were used for processing the natural variations in the E_y and H_x components for the AMT sounding problem. The apparent resistivities ($\rho_{T,\mathrm{AMT}}^{YX}$) and phases ($\varphi_{Z,\mathrm{AMT}}^{YX}$) are imaged as the background in Fig. 8 without averaging. The long-period (right-hand) branches of the resistivity and impedance phase curves were supplemented with the MT sounding data in a neighboring point B-46 of the BEAR network [Varentsov et al., 2002]. The BEAR data are shown in Fig. 8 after the rotation of the matrix of the tensor impedance by 45° into a diagonal position. We generally see good agreement between the CSMT and AMT–MT data. However, we should note at the same time that CSMT data remain more stable in amplitude and shape, although they are spaced 102 km apart from one another. This provides important support to the fact that the choice of the Pnn and Porosozero sites was correct and these stations are located in a similar geologic and tectonic environment, namely, within the ancient Karelian megablock.

It is apparent in Fig. 8 that within the middle frequency band (1–30 Hz) the values of ρ_a^{Zyx} and ρ_a^{Ey} coincide. The spread in values does not exceed 10–20%. At lower frequencies (below 1 Hz), the curves of apparent resistivity diverge due to the near–field influence. At higher frequencies (above 30 Hz), these

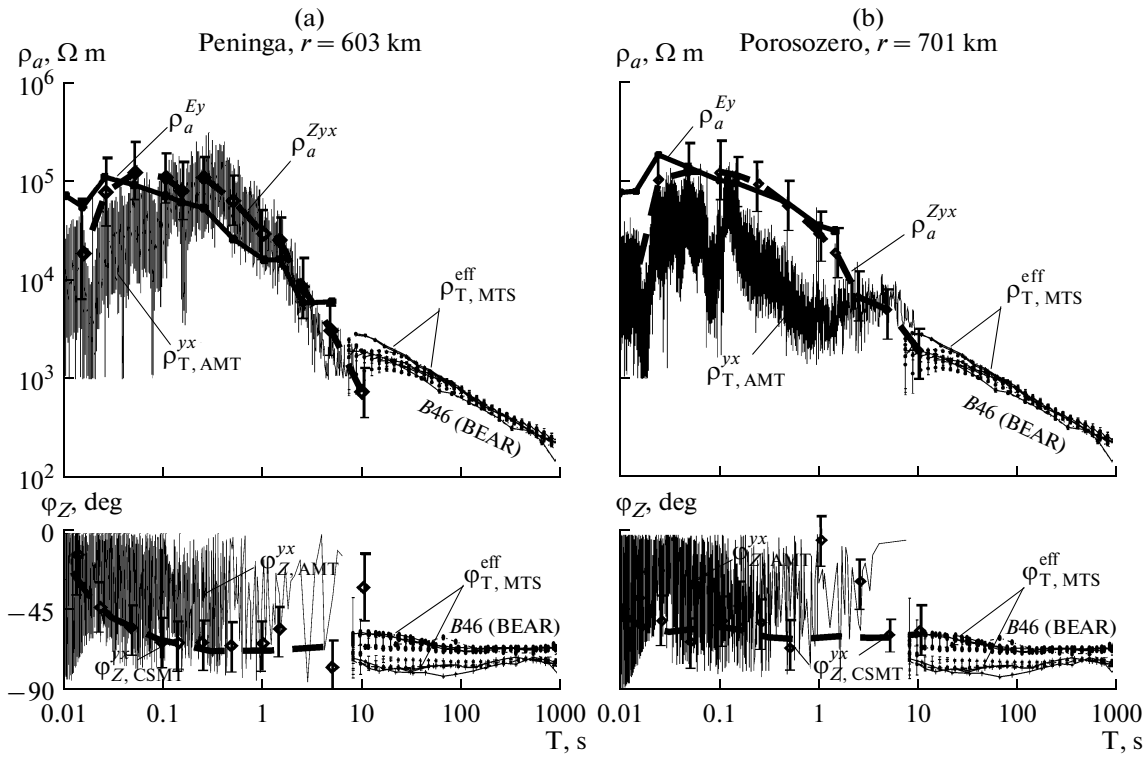

Fig. 8. The processing results of the CSMT sounding data in the field of the industrial PTL L1 at Peninga (a) and Porosozero (b) and the processing results of the AMT–MT sounding data in natural fields (the measurements were conducted using the SChZ-2002 station, GI KSC RAS). The symbols on the curves are ρ_a^{Zyx} and φ_Z^{yx} are the curves of apparent resistivity and impedance phase measured in the field of the L1 sublitudinal line; ρ_a^{Ey} are the apparent resistivity curves for the electric component; E_y; $\rho_{T,AMT}^{yx}$ and $\varphi_{Z,AMT}^{yx}$ are the apparent resistivity and phase impedance curves measured in the field of AMT–MT variations; $\rho_{T,MTS}^{eff}$ and $\varphi_{T,MTS}^{eff}$ are the effective MTS curves of apparent resistivity and phase impedance at point B-46 of the BEAR experiment. Locations of the L1 line and Penning (Pnn), Porosozero (Prs), and B-46 measurement sites are shown in Fig. 3a.

curves diverge due to the influence of the ionosphere and bias currents on ρ_a^{Ey} [Zhamaletdinov et al., 1999]. The effect of bias currents at low frequencies (100 Hz and higher) is revealed because the skin depth in the air in this case is 500 km at most, which is of the same order of magnitude as the distance between the source and the receiver.

The coincidence between the apparent resistivities in the input impedance ρ_a^{Zyx} and in the electrical component ρ_a^{Ey} is an important criterion indicating that (1) the calibration of measuring channels is highly reliable, (2) the far-field conditions (a plane nonuniform wave) are met within the corresponding frequency band and at a given distance [Veshev, 1980; Wait, 1982], and (3) the geoelectric cross section is one-dimensional and the parameters of the lower half-space under the transmitter and the source are similar [Dreizin and Shamraev, 1986].

In order to verify the experimental results described above (Fig. 8), we present below the results of theoretical solution of the forward problem for the field generated by the electric dipole for the considered setups above a layered model of the normal cross section. The cross section shown in Fig. 9a was determined by solving the inverse problem of the FENICS experiment for the given region. The calculations were performed for the input impedance (ρ_a^{Zyx}) and the latitudinal component of the electric field (ρ_a^{Ey}) at distances of 200, 400, and 700 km from the source for a dipole equatorial setup. This scheme approximately corresponds to the sounding in the field of the L1 latitudinal power line in the FENICS experiment. The calculations allow for ionospheric effects and the bias currents. The ionospheric parameters correspond to the nighttime: the resistivity of the ionosphere is $\rho = 10^5$ Ω m, the thickness of the ionospheric layer is 2 km, and the height of the ionosphere above the surface is 150 km [Maeda and Matsumoto, 1962]. The analysis of the theoretical curves shows that the influence of the ionosphere and bias currents results in an anomalous

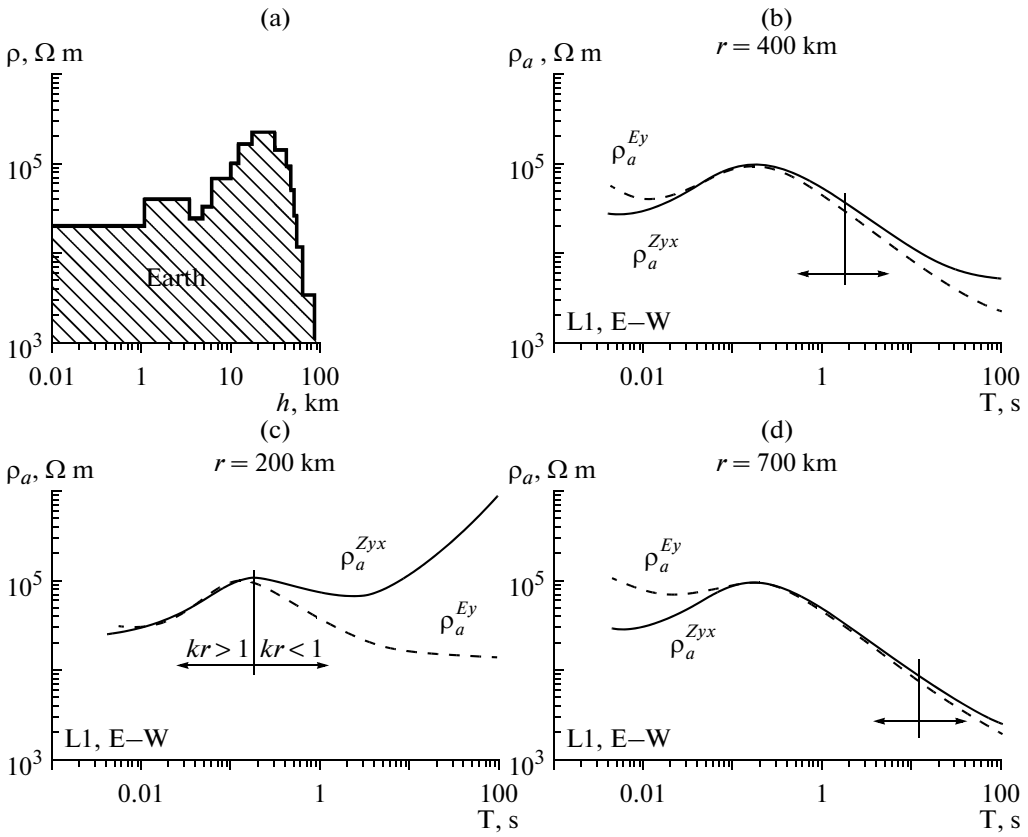

Fig. 9. Theoretical curves of apparent resistivity calculated from the input impedance (ρ_a^{Zyx}) and from the latitudinal electric field component (ρ_a^{Ey}) at distances of 200, 400, and 700 km for a dipole equatorial setup (an analog of the sounding in the field of the L1 latitudinal power line). The model of the lower half-space is shown in Fig. 9a. The vertical line and the horizontal arrows in Figs. 9b, 9c, and 9d mark the boundary between the wave zone ($kr > 1$) and the dc zone ($kr < 1$). The effects of the ionosphere and bias currents were taken into account in the calculations. The ionospheric parameters corresponded to the nighttime conditions ($r = 10^5$ Ω m, the thickness of the ionosphere is 2 km, the height above the surface is 150 km [Maeda and Matsumoto, 1962]).

increase in the apparent resistivity for the electrical component ρ_a^{Ey} with increasing frequency, while the apparent resistivity curves corresponding to the input impedance ρ_a^{Zyx} are not distorted by the effects of the ionosphere and bias currents according to the boundary conditions of M.A. Leontovich: in the wave zone, the values of ρ_a^{Zyx} depend only on the properties of the underlying half-space.

An issue of key importance in the analysis of CSMT soundings is the question about the boundaries of the wave zone. This boundary can be traced by the coincidence of the apparent resistivities calculated from the impedance ρ_a^{Zyx} and from the electrical component ρ_a^{Ey} (Fig. 8). In addition, the wave zone can be outlined by the value of the wave parameter kr, where r is the distance between the transmitter and the receiver and k is the wave number ($k = \sqrt{i\omega\mu_0/\rho}$). The boundary determined by substituting the values of the apparent resistivity at the corresponding frequency to the equation for the wave number k is outlined in Fig. 9 by the vertical bars. The region where $kr > 1$ corresponds to the wave zone, while the area where $kr < 1$ corresponds to the dc zone.

An auxiliary method to trace the configuration of the wave zone and to capture the probable influence of the lateral inhomogeneity of the medium is the analysis of the sounding curves measured for two mutually-orthogonal polarizations of the primary field. In the FENICS-2007 experiment, such measurements were carried out at three stations, namely, Peninga (Pnn), Kostomuksha (Kst), and Tungozero (Tnz). The processing results for these data are presented in Fig. 10a as the apparent resistivity curves calculated from the input impedance. It is apparent that with the increasing distance between the source and the receiver the ρ_a curves of the equatorial (line L1) and axial (line L2) sounding diverge at low frequencies (8 Hz with a spacing of 379 km, station Tnz; 2 Hz with a spacing of

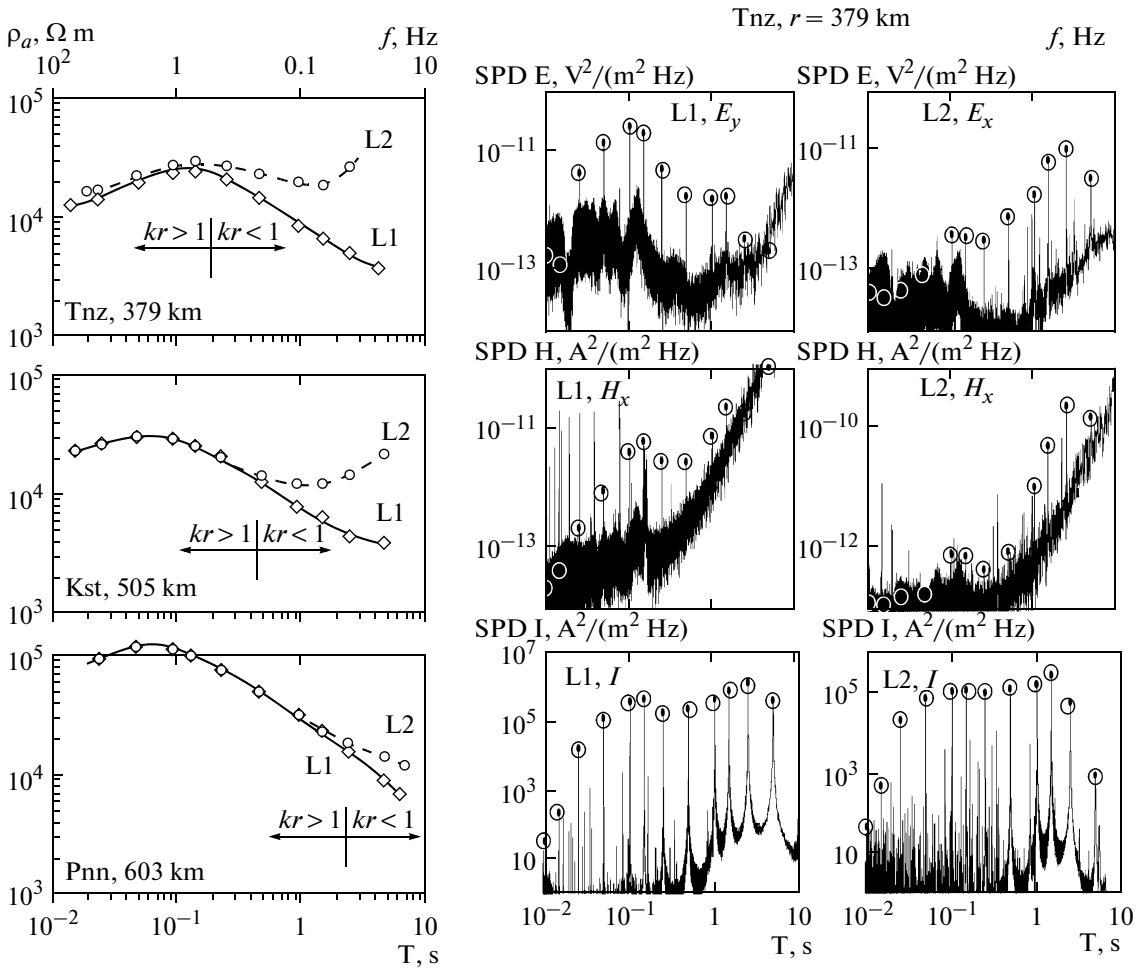

Fig. 10. Experimental CSMT curves of apparent resistivity for the input impedance at Tnz, Kst, and Pnn in the field of the L1 and L2 lines (a) and spectral power density (SPD) of electric and magnetic components in the field of the L1 and L2 lines at Tnz and the corresponding SPDs of the current intensity I in the L1 and L2 lines (b). The L1 sublatitudinal line generates the field in the equatorial setup, and the L2 submeridional line generates the field in the axial setup. The measurements were carried out using SChZ-2002 station of GI KSC RAS. The locations of the power lines are shown in Fig. 3a. Other symbols are the same as in Fig. 9.

505 km, station Kst, and 0.5 Hz with a spacing of 603 km, station Pnn). Note that the coordinates of the divergence points of the curves exactly coincide with the boundaries of the wave zone numerically estimated for each point from the parameter kr (Fig. 10a).

The pattern of variations in the apparent resistivity curves associated with the changes in orientation of the primary field, which can be seen in Fig. 10a, is illustrated in Fig. 10b by the graphs of SPD of the electric and magnetic components for the measurements carried out at Tnz, $r = 379$ km. We see in Fig. 10b that the frequency dependence of SPD of the current strength in L1 and L2 lines is similar, although the frequency dependences of SPD of the electric and magnetic field components when switching the L1 or L2 line substantially differ and coincide with the pattern of the corresponding apparent resistivity curves. The behavior of the electric field is the most illustrative. When the latitudinal L1 line is switched on, the electric field E_y decreases with decreasing frequency and, as a result, the values of ρ_a^{Zyx} also decrease with decreasing frequency (Fig. 10a). When the submeridional L2 line is switched on, the E_x field increases with decreasing frequency and, correspondingly, ρ_a^{Zxy} increase, too (Fig. 10a).

The characteristic features in the behavior of experimental curves of apparent resistivity are in perfect agreement with the theoretical estimates. According to [Veshev, 1980], the electric field of an earthed dipole for the equatorial (E_θ) and axial (E_r) arrangements is described by the equation $E_{\theta,r} = E^0 e_{\theta,r}$, where $E^0 = \dfrac{\rho_1 IAB}{2\pi r^3}$ is the dc dipole field and $e_{\theta,r}$ is the electric number reflecting the frequency dependence of the field.

For the equatorial setup, $e_\theta = 2 - (1 + kr)e^{-kr}$.

For the axial setup, $e_r = 1 + (1 + kr)e^{-kr}$.

It is common practice in the theory of frequency sounding to normalize the field by the field of the wave zone [Vanyan, 1965]. In this case, the curves of apparent resistivity above the layered half-space coincide for the axial and equatorial setups. With the decrease in frequency and attaining the dc region, the values of apparent resistivity for the equatorial setup halve, while those for an axial setup double. These theoretical estimates are supported in the experiment, which is seen in Fig. 10a.

When analyzing the above situation as applied to the apparent resistivity curves for the input impedance, it is necessary to take into account the behavior of magnetic components. Confining ourselves to the analysis of the wave zone, we give the expressions for the electric and magnetic field components of a horizontal electric dipole oriented along the X axis according to the data of [Veshev, 1980] (conversion from CGS to SI taken into account):

$$E_x = \frac{IL_{AB}(3\cos^2\theta - 2)}{2\pi r^3}\rho,$$

$$H_y = -\frac{IL_{AB}(3\cos^2\theta - 2)}{2\pi r^3\sqrt{i\omega\mu}}\sqrt{\rho},$$

where I is the current strength in amperes, L_{AB} is the length of the dipole AB in meters, ρ is the electric resistivity in Ω m, r is the spacing in meters, θ is the angle between the dipole axis and the direction to the receiving point, $\omega = 2\pi f$ is the angular frequency in radians, and $\mu_0 = 4\pi \times 10^{-7}$ [H/m] is the magnetic permeability of free space.

It is apparent from the above expressions that the intensity of the magnetic field depends on the resistivity of the medium (which enters in the radicand) and, thus, the properties of the field at the transition from a wave zone to a dc zone are mainly determined by the electric components of the input impedance field.

In order to verify the experimental results shown in Fig. 10, we theoretically calculated the apparent resistivity curves of an electric dipole from the input impedance at distances of 200, 400, and 700 km from the source for the equatorial arrangement scheme (which is an analog to the sounding in the field of the latitudinal line L1) and for the axial setup (an analog to the sounding in the field of the meridional line L2). The results of calculation are presented below in Fig. 11.

Comparison of Fig. 10a and Fig. 11 shows the complete agreement between the experimental and theoretical data. The curves in Fig. 10a and Fig. 11 are so close to each other that one might assume that the measurements have been made in an electrolyte bath rather than in a real structurally and compositionally inhomogeneous geological medium. One important feature is worth noting in the behavior of the apparent resistivity curves for the equatorial setup: according to both the experimental and theoretical data, these curves are descending over the entire frequency range spaced in excess of 400 km apart from each other. It indicates that wave zone conditions are valid up to the lowest frequencies. The observed phenomenon can be associated, first of all, with a gradient increase of the lithosphere electric conductivity with depth starting from 15–20 km and below. As a result, with decreasing frequency the electromagnetic field generated by L1 (the equatorial setup) penetrates deeper into the rocks with higher conductivity. Due to this fact, the wavelength of the electromagnetic wave in the lithosphere only faintly increases with decreasing frequency, and the field within the entire low-frequency range remains in the wave zone conditions. In case of sounding with the L2 line (the axial setup) this effect is either weaker or scarcely observed at all since the depth of axial sounding is twice as low as that in case of equatorial sounding [Zaborovsky, 1963; Spice, 1989]. We should also take into account that the center of the L2 line is 50 km nearer to the sounding points on the meridional profile than the center of the L1 line. It also reduces the depth of sounding with the L2 line.

The aforementioned features of the equatorial and axial setups (Figs. 8–11) revealed in the data of the FENICS-2007 experiment were confirmed by the results of the FENICS-2009 experiment. Figure 12 exemplifies the results of measurements made in 2009 at the Popov Porog station (point 13 in Fig. 3) using the GI MTS-1 station (St. Peterburg Branch of IZMIRAN).

The data were processed in terms of the total electric field. Figure 12 clearly demonstrates the coincidence of the equatorial ($\rho_a^{E\text{tot}}$, L1) and the axial ($\rho_a^{E\text{tot}}$, L2) curves of apparent resistivity in the wave zone over the frequency band 1–10 Hz. Below 1 Hz we observe a sharp ascent in the apparent resistivity curve $\rho_a^{E\text{tot}}$, L2 for the axial setup, which indicates the termination of the wave zone conditions. The same data were used in MTS processing for the Popov Porog site using the modified program by V.Yu. Semenov. The MTS data are in good agreement with the CSMT results at the maximums of the sounding curves but substantially deviate toward anomalously high values of apparent resistivity at the frequencies of 2–0.2 Hz.

It can be assumed that the discrepancies in CSMT and MT–AMT data apparent in Figs. 8 and 12 are related to the insufficient time of accumulation of MT–AMT variations. Thus, we can conclude that it is sufficient to increase the observation time in natural fields to ensure the complete coincidence of the results. However, the example of the comparison of the MTS and CSMT results for the Pertozero station (Fig. 13) presented below casts doubt on such an assumption. Continuous measurements at Pertozero were conducted for 7 days. Night signals from the sublatitudinal power transmission line L1 were recorded each day against the MT variations. Measurements were carried out using the GI-MTS-1 station (the Institute of Physics at St. Petersburg State University) with torsion magnetometers in the frequency range of 0–8 Hz with the sampling frequency of 50 Hz. The data processing results are shown in Fig. 13.

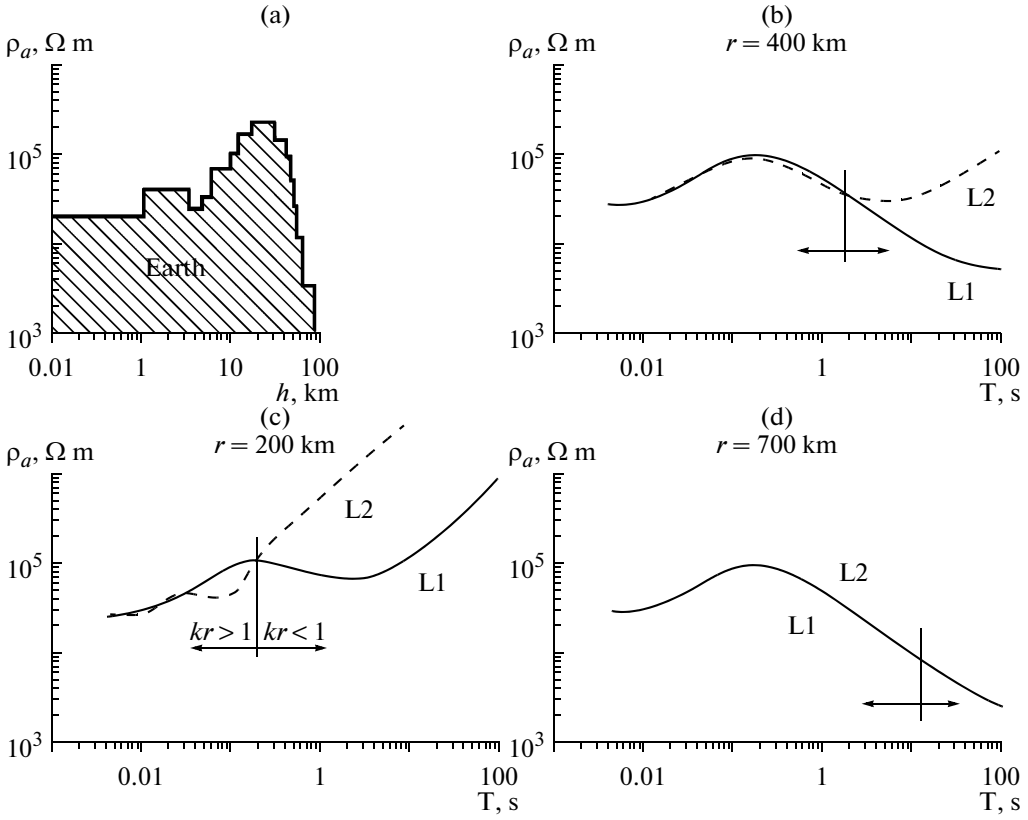

Fig. 11. Theoretical CSMT apparent resistivity curves calculated from the input impedance at distances of 200, 400, and 700 km from the source for the equatorial dipole setup (L1) and for the axial dipole setup (L2). The locations of the L1 and L2 lines are shown in Fig. 3a. Other symbols are the same as in Fig. 9.

The curve ρ_T^{MTS} in Fig. 13 is obtained by summation of the MTS data for all 7 days. The processing was performed in accordance with the Semenov's program. The values of ρ_T^{MTS} correspond to the effective values. The results of CSMT sounding in the field of L1 line for all 7 night recording sessions were also summed up. Here, we used the total impedance values because the amplitudes of both horizontal components of the electric and magnetic fields were nearly similar in spite of the fact that the receiving point lay on the equatorial axis of the current dipole of L1 (Fig. 3). This can be indicative of the local horizontal inhomogeneity of the medium in the vicinity of the Pertozero observation point. A possible reason could be the location of the observation point on the axis of an extended fault. This fact can also explain why the CSMT sounding curve lies about half an order of magnitude lower than the normal curve of apparent resistivity observed in most CSMT sounding points within the Karel megablock. But the left-hand high-frequency branch of the MTS curve has an even lower position. Formal interpretation of this curve based on the *S*-asymptotics reveals a conductive layer with the longitudinal conductivity on the order of 5 S in the upper part of the cross section. This conclusion is inconsistent with the concept of the geoelectric section in this region based on the results of sounding with ac and dc controlled sources. According to the latter, the longitudinal conductivity of the sedimentary cover (moraine) in this region is hundredths of fractions of Siemens, and the intermediate conducting *DD* layer revealed at depths of 2–10 km, as estimated earlier [Zhamaletdinov, et al., 2005] and will be shown below in Fig. 14, has a longitudinal conductivity of tenths of fractions of Siemens.

A GEOLOGICAL–GEOPHYSICAL INTERPRETATION OF THE FENICS RESULTS

The basic data for the complex geological–geophysical interpretation of the FENICS experiments were the results of CSMT sounding along the 700 km-long Upoloksha–Porosozero submedirional profile. The results of preprocessing the data for the profile and their one-dimensional inversion are shown in Fig. 14.

The distances between the measuring stations and the L1 and L2 transmitting antennas vary from 186 km (Upl) to 701 km (Prs). The main information about the deep cross section were obtained from the results of sounding in a low-frequency range of 0.1–200 Hz. Along with it, the high-frequency (f > 1000 Hz)

branches of the apparent resistivity curves, which contain information about the uppermost near-surface portions of the geoelectric cross section, were also calculated. These data were obtained by the recalculation of the apparent resistivity curves of the dc sounding in the frequency domain. The dc sounding was carried out at each point of the CSMT measurements. The distances between the transmitter and the receiver varied from 2 to 10–15 km. All dc soundings were conducted in two mutually orthogonal directions in order to study the probable effects of anisotropy. In most cases the anisotropy factor $\lambda = \rho_a^{max}/\rho_a^{min}$ did not exceed 1.2. The apparent resistivity curves were converted into the frequency domain in two stages. At the first stage, the dc apparent resistivity curves were inverted into 1D resistivity models of the lower halfspace. At the second stage, a forward one-dimensional problem of frequency sounding in the far zone was solved for the resistivity model of the upper crust yielded by the dc sounding. Then, a high-frequency branch of the apparent resistivity curve obtained in the dc sounding was interpolated using the data of CSMT sounding in the field of industrial PTLs (curves 4 in Fig. 14a).

The apparent resistivity curves in Fig. 14a have similar shapes. This indicates that there are common features in the depth distribution of resistivity persisting along the entire 700-km-long profile. In particular, in all curves the resistivity decreases at about 100 Hz, which is related to the inhomogeneity of the intermediate conducting region, the DD layer, at a depth ranging from 2–3 km to 5–10 km [Zhamaletdinov et al., 2005]. All CSMT sounding curves have a broad maximum in the vicinity of 5–10 Hz with the apparent resistivity attaining 30 to 100 thousands Ω m. It is worth noting that the apparent resistivity curves are in good agreement in spite of the fact that the measurements were carried out in different years, at different stations, and with different sources. The signals transmitted by the L1 and L2 lines were measured a week apart with totally new configurations of electric lines and magnetic sensors. Circles no. 4 mark the points of sounding with the Zevs ULF antenna (line L3 in Fig. 3) carried out in 2008. They also agree well with the other data.

The problem of the inversion was solved for the input impedance apparent resistivity curves. The solution of this problem was based on the solution of the forward problem for the field of a horizontal electric dipole in a horizontally-layered medium. The program was developed by A.N. Shevtsov [2001; 2006] based on the theoretical concepts presented in [Chave, 1983; Chave, 1984; Boerner, 1991]. The source and the receiving points are described by the spherical coordinates (r', φ', z') and (r, φ, z), respectively. The entire medium is assumed to be horizontally-layered, and the kth layer has the following parameters: σ_k is the conductivity, ε_k is the absolute dielectric permittivity, μ_k is the absolute magnetic permeability, and h_k is the power. The field components in a layered medium are determined by the following expression:

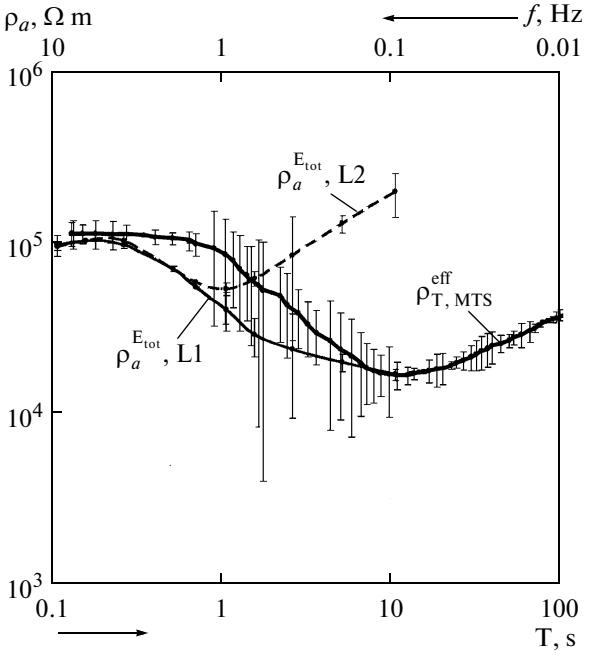

Fig. 12. The results of CSMT sounding with L1 and L2 industrial power transmission lines at the Popov Porog station ($r = 635$ km) compared to the data of the AMT–AM sounding at the same point: ρ_a^{Etot}, L1 is the CSMT curve calculated from the total electric field (L1, the equatorial setup); ρ_a^{Etot}, L2 is the same for L2, the axial setup; $\rho^{eff}_{T, MTS}$ is the MTS curve obtained from the total field. The locations of L1, L2 and the Popov Porog station (13) are shown in Fig. 3a. The measurements were carried out using the GI-MTS-1 station, SPbPIZMIRAN.

$$\begin{bmatrix} E_x \\ E_y \\ E_z \\ B_x \\ B_y \\ B_z \end{bmatrix} = \frac{I(\omega)}{4\pi}\int_0^{\infty}\tilde{F}\begin{bmatrix} \partial_{xx} \\ \partial_{xy} \\ \partial_x \\ \partial_y \\ 1 \end{bmatrix}\lambda J_0(\lambda\xi)d\lambda,$$

where $I(\omega)$ is the source current depending on the circular frequency, $J_0(\lambda\xi)$ is the Bessel function of the first kind of a zero series, $\xi = \sqrt{r'^2 + r^2 - 2rr'\cos(\varphi' - \varphi)}$ is the distance between the source and the receiver on the projection to a horizontal plane, and $\tilde{F}$ is the universal parent matrix (6×5).

On the basis of this forward problem solution, we carried out all numerical calculations shown in Figs. 8 and 12. The same solution of the forward problem was also used for the inversion of the data in terms of the total field without dividing it into far, near, and intermediate zones. The inversion itself was carried out using three different methods, namely, based on the method of effective lineariza-

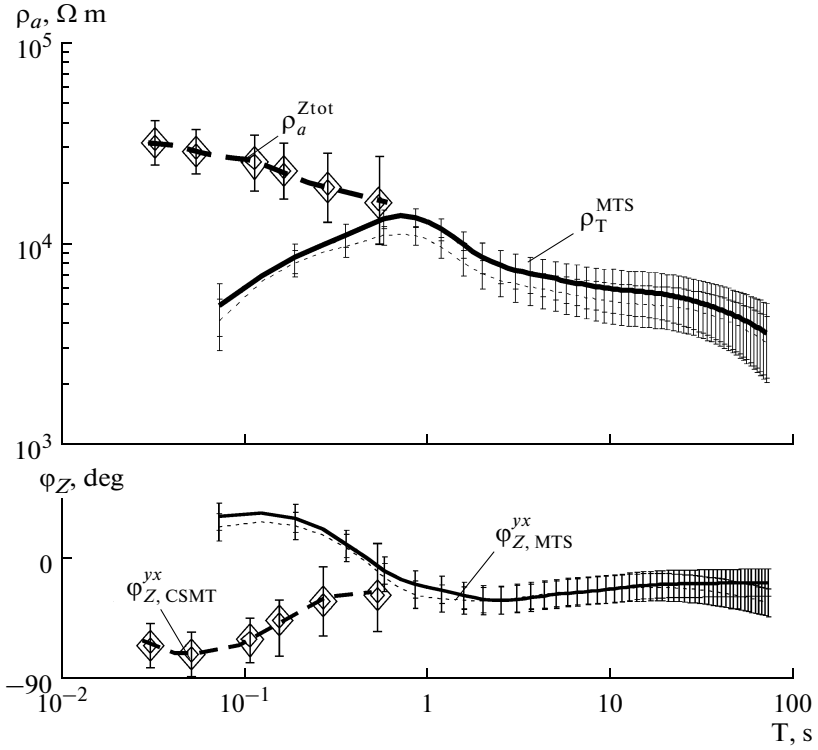

Fig. 13. Comparison of the results of CSMT sounding in field generated by the L1 line and the MTS results at Pertozero station ($r = 570$ km): ρ_a^{Ztot} is the CSMT apparent resistivity in the L1 field calculated from the total impedance; $\varphi^{YX}_{Z,\,CSMT}$ is the same, the *YX* impedance phase; $\rho^{eff}_{T,\,MTS}$ and $\varphi^{YX}_{Z,\,MTS}$ is the effective apparent resistivity and *YX* impedance phase according to MTS. The measurements were carried out using GI-MTS-1 station, SPbSU. The location of Pertozero station (Prt) and L1 line are shown in Fig. 3a.

tion (MEL) [Porokhova and Kharlamov, 1999], the controlled transformation technique [Berdichevsky and Dmitriev, 1991], and the standard fitting method [Berdichevsky and Dmitriev, 1991]. The latter turned out to be the most efficient for bimodal interpretation. All inversions were carried out for the phase data. The phases were calculated from the apparent resistivity curve in accordance with the Weidelt formula and played a supportive role as an indicator of smoothness of the apparent resistivity curve.

One-dimensional resistivity cross sections yielded by inversion are shown in Fig. 14b. The bimodal inversion using both polarizations of L1 and L2 fields was carried out for three sites where the signals from L1 and L2 power transmission lines (Tng, Kst, Prs) were measured. The agreement between the results of the bimodal inversion and the experimental data measured with two quasi-orthogonal polarizations of the primary field is another important argument in favor of the homogeneous (one-dimensional) structure of the deep electric conductivity of the lithosphere of Eastern Fennoscandia.

The general analysis of the results of deep electromagnetic soundings carried out in the scope of the FENICS experiment allows us to make the three following main conclusions.

1. There is complete agreement (in shape and in amplitude) between the apparent resistivity curves over the eastern part of the Baltic shield, including the 700 km-long submeridional profile.

2. There is a coincidence (within 10–20% error) of the apparent resistivity curves calculated from the electric component and from the input impedance as well as the apparent resistivity curves measured with latitudinal and meridional polarizations of the primary field within the wave zone.

3. There is an agreement between the experimental and theoretical estimates of the boundaries of the wave zone and its manifestations in the apparent resistivity curves CSMT sounding with the axial and equatorial arrangement of the current and receiving lines.

Taken together, the aforementioned analysis of the raw data of deep sounding (Figs. 8, 10, 12, 13, and 14a), the theoretical calculations (Figs. 9 and 11), and the inverse problem solutions (Fig. 14b) suggest the main conclusion that the deep structure of the electric conductivity distribution in the lithosphere of the eastern part of the Baltic shield is characterized by substantial horizontal inhomogeneity (stratification) of the electric properties within the depth range from 15–20 to 50–70 km. This conclusion contradicts the multi-year experience of the magnetotel-

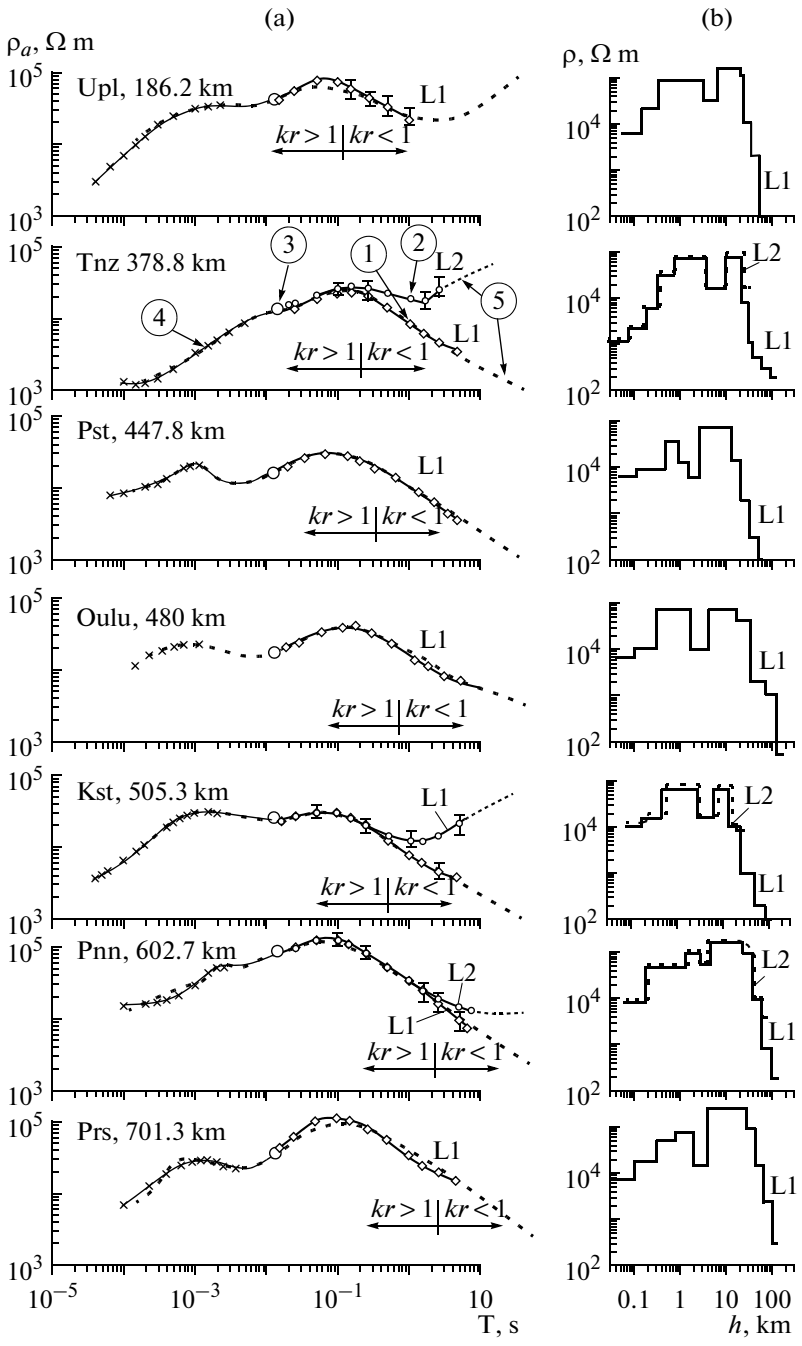

Fig. 14. A combined diagram of the results of CSMT sounding at the 700 km-long Upolaksha–Porosozero profile: (a) apparent resistivity curves; (b) one-dimensional cross sections $\rho(h)$ reconstructed from the results of the inverse problem solution. Legend: the figures in circles are given for Tnz, $r = 378.8$ km: (1) ρ_a^{Zyx} curve in the field generated by L1 line; (2) ρ_a^{Zxy} curve in the field generated by L2 line; (3) ρ_a^{Zyx} curve in the field generated by L3 line at a frequency of 82 Hz; (4) ρ_ω curve of frequency sounding calculated theoretically from the data of dc sounding with spacings up to 10 km; (5) theoretical ρ_a curves calculated from the results of inverse problem solution. The locations of the L1, L2 lines, and the sounding stations are shown in Fig. 3a.

luric investigations, including the MTS results cited in the present paper, that point to a sharply contrasting electric inhomogeneity of the Baltic shield lithosphere [Rokityansky et al., 1963]. This inconsistency needs further research.

Against the generally homogeneous background geoelectric cross section of the Baltic shield lithosphere in the northwestern part of the Karelian megablock and in Finland (the region of Oulu), there is a region where the apparent resistivity curves are dis-

Table 2. Transverse resistance of the lithosphere according to the FENICS experiment

Point	$T = \sum h_i \rho_i$, 10^9 Ω m^2	Distance, km
Upl	4.0	186
Tnz	1.2	379
Pst	0.8	448
Oulu	1.4	480
Kst	0.8	505
Tgd	11.2	510
Pnn	5.2	603
Prs	7.6	701

placed downward to a lower level of resistivity (Fig. 14a) and, hence, the transverse resistance of the lithosphere is also reduced over an area as large as about 80 thousand km^2. The transverse electric resistance **T** is determined as $\mathbf{T} = \sum_{i=1}^{i=n} h_i \rho_i$, where h_i is the thickness and ρ_i is the resistivity of the *i*th layer in the lithosphere at depths of 10–50 km (See Table 2).

The background (normal) value of the transverse lithosphere resistance is estimated to be on the order of 10^{10} Ω m^2. Note that this value coincides with the estimation based on the data of the Khibiny experiment with the MHD facility [Zhamaletdinov, 1990] and is close to the average transverse resistance of the continental crust derived in [Fainberg et al., 1990] from the data on solar daily variations (3×10^9 Ω m^2). Within the limits of the anomaly, the transverse resistance reduces to 10^9 Ω m^2. The configuration of the anomaly is shown in Fig. 15a in the isolines of **T**.

The comparison of the shape of the transverse resistance anomaly with the schematic distribution of the crustal conductive bodies [Zhamaletdinov, 1990; Korja et al., 2002] reveals no common features between them (see Fig. 15b). This inconsistence indicates the deep location of the anomaly in the transverse resistance since by their nature the crustal anomalies are completely determined by the effects of the electronically conductive sulfide–carbonaceous rocks in the near-surface layer [Zhamaletdinov, 1990].

In Fig. 16a the configuration of the anomaly in the transverse resistance of the lithosphere **T** is compared with the generalized geological map of the study region [Pozhilenko et al., 2002]. However, again in this case we do not observe any correlation between the location of the T anomaly and the surface geology map. On the other hand, in Fig. 16b it is apparent that the **T** contours agree well with the location of the Moho anomaly determined from the seismic data in Central Finland [Pavlenkova, 2006]. On the northeast, the *1a* contours outline a vast region of the Moho deepening to a depth of 60 km. Note that, in accordance with the seismic data, the crustal thickness over the major part of the Baltic shield is not larger than 37–40 km.

The apparent resistivity curves averaged over the whole volume of the above described data for the normal and anomalous lithospheric cross sections of the eastern part of the Baltic (Fennoscandian) shield are shown in Fig. 17, on the left. These curves are marked as *1a* and *2a*, respectively. The results of the inverse problem solution for the normal and the anomalous sections (curves *1b* and *2b*, respectively) are shown on the right-hand side of Fig. 17. The maximal drop in resistivity in cross sections *1b* and *2b* occurs at a depth of 20 km where the resistivity of 300–400 thousands Ω m in the normal region reduces to about 100 thousand Ω m in the anomalous region. On the whole, the region with reduced resistivity of the lithosphere in the anomalous zone corresponds to the depth interval from 10 to 40 km.

The nature of the decrease in resistivity of the lithosphere in the anomalous region seems to be due to the impurity conductivity associated with the lattice defects, while free fluids are likely absent or negligible because of the high general resistance of the material, namely, 100 thousand Ω m and higher. The impurity conductivity has a semiconductor nature. The electric current can be carried by both negative charges (electrons) and positive holes [Zharkov, 1983]. The pattern of the observed anomaly also depends on the temperature, which increases with depth. The temperature dependence of resistivity of semiconductors is usually described by the exponential law [Ioffe, 1974]

$$\rho = \sum_{i=1}^{i=n} \rho_0^i e^{E_0^i / k^0 T},$$

where ρ_0^i is the preexponential coefficient numerically equal to the resistivity of the *i*th carrier of electricity at ${}^0T \longrightarrow \infty$ [Parkhomenko, 1982], E_0^i is the activation energy in electron volts, k is the Boltzmann constant (1.38×10^{-23} J/K), and ${}^0T$ is the Kelvin temperature.

The geoelectric sections shown in Fig. 17 can be used in the modeling of the rheology of the lithosphere. This modeling is based on the above-described methods of geothermal interpretation of the deep geoelectric data and on the results of laboratory testing of the electric conductivity of rock specimens under high thermodynamic parameters [Parkhomenko and Bondarenko, 1972]. We describe here the first experience in such calculations based on application of the Coulomb law at relatively low temperatures $T < 0.5T_s$, where T_s is the melting temperature. In this case, $\sigma_1 - \sigma_3 \geq \beta(1-\theta)P(z)$, where $\sigma_1 - \sigma_3$ is the difference between the maximal and minimal compressive stresses, $P(z)$ is the lithostatic pressure, β is the coefficient of static friction, and θ is the ratio of the pore pressure to the lithostatic pressure. At high temperatures $T > 0.5T_s$ in the yield strain region, we used the equation of the steady-state creep (dislocation creep)

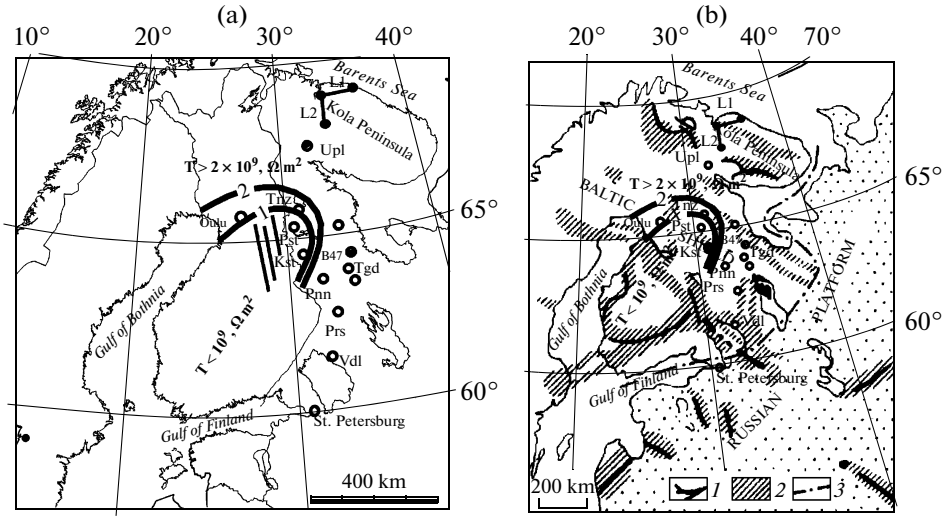

Fig. 15. The isolines of transverse electric resistance of lithosphere **T** in $\Omega\ m^2$ (a) and its comparison with the distribution of the crustal anomalies of electric conductivity (b) [Zhamaletdinov, 1990; Korja et al., 2002]. (*1*) The axes of the electric conductivity anomalies, S ≥ 1000 s; (*2*) Regions with reduced crustal resistance, $S = 10–100$ S; (*3*) The boundary between the Baltic shield and the Russian platform.

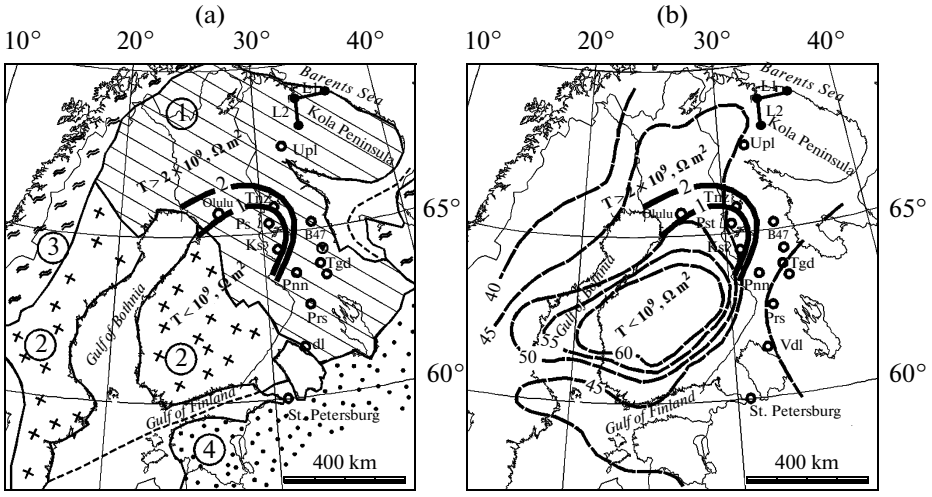

Fig. 16. Isolines of the transverse lithospheric resistance **T** calculated from the data of the FENICS experiment and comparison with the geological map (a) [Pozhilenko, 2002] and the Moho map according to seismic data (b) [Pavlenkova, 2006]. (*1*) Archaean complexes; (*2*) Svecofennian protertzoic complex; (*3*) caledonites; (*4*) sedimentary cover of the Russian Platform; (b) contours of the Moho's depths are in kilometers.

$$\sigma_1 - \sigma_3 = \left(\frac{\dot{e}}{A}\right)^{1/n} \exp\left(\frac{E}{nRT(z)}\right),$$

$$\sigma_1 - \sigma_3 = \sigma_D\left(1 - \left(-\frac{RT}{E_D}\ln\left(\frac{\dot{e}}{A_D}\right)\right)^{1/2}\right).$$

where $\dot{e}$ is the strain rate, R is the gas constant, E is the activation energy, $T(z)$ is the temperature at depth z, and A and n are the constants for a given type of geological material.

In the lower part of the geoelectrical cross section in Fig. 17, an expression for the Dorn law was used for olivines under high pressure (above 200 MPa) [Kaikkonen et al., 2000]

The strain rate was assumed to be $\dot{e} = 3 \times 10^{-15} s^{-1}$. Other calculation parameters were taken from Table 1 in [Kaikkonen et al., 2000].

The results of modeling the rheological characteristics of the lithosphere for the measured curves of apparent resistivity are presented in Fig. 18. The calculations were carried out for two types of a normal section. The type I

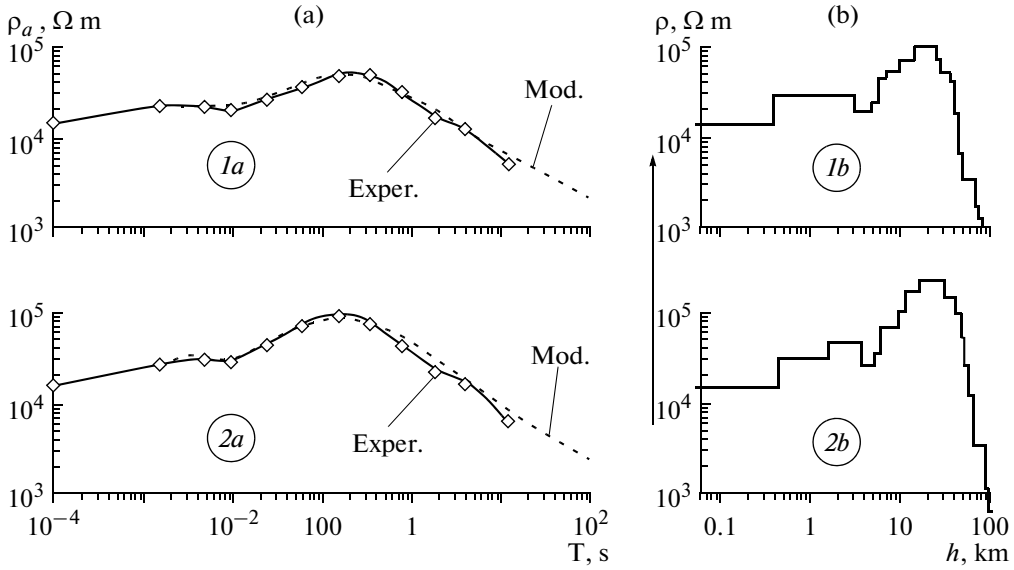

Fig. 17. Apparent resistivity curves (a) and cross sections (b) according to the results of CSMT sounding in the northeast part of the Baltic shield for the lithosphere with normal ($\mathbf{T} \geq 2 \times 10^9$ Ω m^2, Figs. 1a and 1b) and anomalous ($\mathbf{T} \leq 10^9$ Ω m^2, Figs. 2a and 2b) types of cross sections shown in the **T** isolines in Figs. 15 and 16. The marks "Exper" and "Mod." on the curves stand for "experimental" and model (theoretical)], respectively.

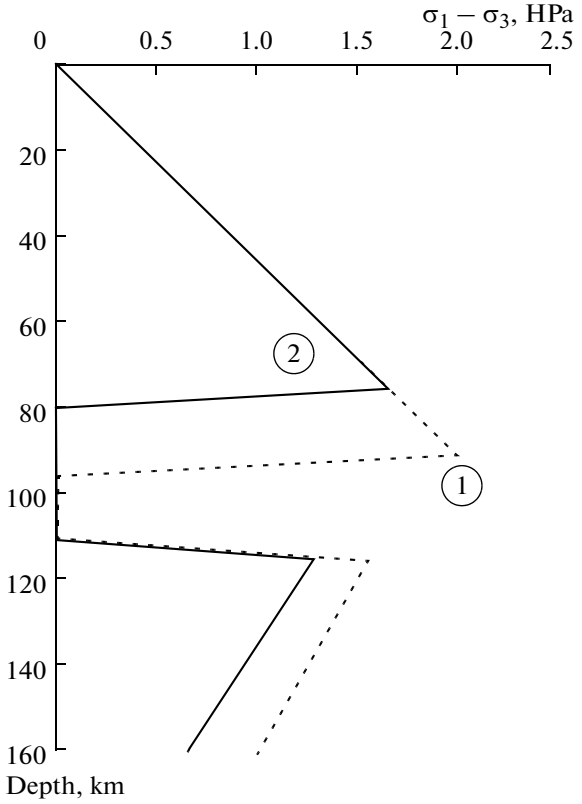

Fig. 18. Rheological profiles of the eastern part of the Baltic shield according to the geoelectric results of the FENICS experiment.(1) A rheological profile for a normal cross section (*1b* in Fig. 17); (2) The same for an anomalous cross section (*2b* in Fig. 17). The locations of regions with normal and anomalous geoelectric cross sections of the lithosphere are shown in Figs. 15 and 16 by the isolines of the transverse resistance.

section (conditionally cold) has a transverse resistance of $T = 10^{10}$ Ω m^2. This type of cross section was identified in the eastern part of the Karelian megablock and on the Kola Peninsula (curve *1* in Fig. 17) in accordance with the data of the FENICS experiment. The type II section, which is conditionally heated, is characterized by low transverse resistance $T = 10^9$ Ω m^2. This cross section was revealed from the data of the FENICS experiment in the western part of the Karelian megablock and in central Finland (curve *2* in Fig. 17).

The type II cross section is characterized by a temperature that is 50 degrees higher in the bottom crust and by a shallower upper creep boundary (80 km) than the type I (cold) cross section, where this boundary runs at a depth of 110 km. The region where the differential stress ($\sigma_1 - \sigma_3$, GPa) drops to zero indicates the state of the yield of the material.

The above-presented calculations should be considered as an initial stage of more detailed research to be carried out in the future concerning the implications of the deep geoelectric data in the study of the thermodynamic regime and rheological parameters of the lithosphere. The proposed explanations of the nature of an anomalous decrease in resistivity in the southwest part of the study region are only hypothetic versions based on the physical reasoning. The observed fall in resistivity can also be associated with the change in the composition of the lithospheric material in the anomalous region for a darker-colored rock composition or with the geodynamic phenomena. In any case, the solution to the problem of complex interpretation of geoelectric and seismic data necessitates conducting additional experiments and theoretic calculations.

CONCLUSIONS

1. A unique generator-and-measurement complex for deep sounding of the lithosphere in the frequency range of 0.1–200 Hz is developed and tested. The complex includes the industrial PTLs and the Energy-2 generator supplying power up to 200 kW.

2. The experiments FENICS-2007 and FENICS-2009 on the tensor frequency sounding of the lithosphere are carried out in the eastern part of the Baltic shield at distances of up to 700 km from the source in the frequency range 0.1–200 Hz. Individual measurements of the electromagnetic field generated by the Energy-2 generator in the industrial PTLs have been conducted at distances up to 2150 km from the source.

3. The lithosphere in the eastern part of the Baltic shield at depths from 15–15 to 50–70 km is found to be fairly horizontally homogeneous (stratified).

4. An area with anomalously reduced transverse resistance of the lithosphere is revealed in the northwestern part of the Karelian megablock and in Finland. On the northeast, this area borders the region of the Moho boundary deepening to a depth of 60 km.

5. The parameters of the normal deep geoelectric section of the lithosphere in the northeastern part of the Baltic (Fennoscandian) shield are investigated. Based on the obtained geoelectric cross sections, the rheological parameters of the lithosphere are estimated.

ACKNOWLEDGMENTS

The study was supported by the Russian Foundation for Basic Research (projects nos. 06-07-64429 and 07-08-00181), the Department of Earth Sciences of the Russian Academy of Sciences (project no. 6 "Geodynamics and Deformation Mechanisms of the Lithosphere") and the Academy of Science of Finland (project no. 107424). The participation of the Institute of Radio Astronomy in the experiment was partly supported under the Yatagan, Spitsbergen, and Okruzhenie R&D projects of the National Academy of Sciences of the Ukraine. The authors are grateful to the Chief Engineer of KolEnergo, A.V. Maslov and to the head of the KSR KP MES of the North West, I.G. Reshetnyak for their help in the organization of the work at industrial PTLs, and to the Doctor of Technical Sciences, V.E. Korepanov, for his assistance in the organization of remote signal measurements at the maximal distance of 2150 km.

REFERENCES

Akindinov, V.V., Naryshkin, V.I., and Ryazantsev, A.M., Electromagnetic Fields in Sea Water (A Review), *Radiotekh. Elektron.*, 1976, vol. 21, no. 5, pp. 913—944.

Barannik, M.B., Danilin, A.N., Efimov, et al., High-Voltage Power Inverter of the Generator "Energy-2" for Electromagnetic Soundings and Monitoring of the Earthquake Source Zones, *Seism. Prib.*, 2009, vol. 45, no. 2, pp. 5–23 [*Seismic Instruments* (Engl. Transl.), 2010, vol. 46, no. 1, pp. 49–61].

Berdichevskii, M.N., *Elektricheskaya razvedka metodom magnitotellurichеskogo profilirovaniya* (Electric Survey Using the Method of Magnetotelluric Profiling), Moscow: Nedra, 1968.

Berdichevskii, M.N. and Dmitriev, V.I., *Magnitotellurichеskoe zondirovanie gorizontal'no odnorodnykh sred* (Magnetotelluric Sounding of Horizontally Homogeneous Media), Moscow: Nedra, 1991.

Bernstein, S.L., Burrows, M., Evans, J.E., et al., Long-Range Communication at Extremely Low Frequencies, *Proc. IEEE*, 1974, vol. 62, no. 3, pp. 292–312.

Blohm, K., Worzyk, P., and Scriba, H., Geoelectrical Deep Soundings in Southern Africa Using the Cabora Bassa Power Line, *J. Geophys.*, 1977, vol. 43, pp. 665–679.

Boerner, D.E., Controlled Source Electromagnetic Deep Sounding: Theory, Results and Correlation with Natural Source Results, in *Proc. 10th Workshop on EM Induction*, Ensenada: Mexico, 1991, pp. 3–50.

Cantwell, T., Nelson, P., Webb, J., and Orange, A.S., Deep Resistivity Measurements in the Pacific North–West, *J. Geophys. Res.*, 1965, vol. 70, no. 8, pp.1931–1937.

Chave, A.D., Numerical Integration of Related Hankel Transforms by Quadrature and Continued Fraction Expansion, *J. Geophys.*, 1983, no. 48, pp. 1671–1686.

Chave, A.D.,The Freshet Derivatives of Electromagnetic Induction, *J. Geophys. Res.*, 1984, no. 89, pp. 3373–3380.

Dreizin, Yu.A. and Shamraev, I.M., On The Theory of Electromagnetic Survey with High-Power Sources, *Dokl. Akad. Nauk SSSR*, 1986, vol. 288, no. 4, pp. 837–841.

Fainberg, E.B., Kuvshinov, A.V., and Singer, B.Sh., Electromagnetic Induction in a Spherical Earth with Nonuniform Ocean and Continents in Electric Contact with the Underlying Medium: I. Theory, Method and Example, *Geophys. J. Int.*, 1990, vol. 102, pp. 273–281.

Fainberg, E.B., Kuvshinov, A.V., and Singer, B.Sh., Electromagnetic Induction in a Spherical Earth with Nonuniform Ocean and Continents in Electric Contact with the Underlying Medium: II. Bimodal Global Geomagnetic Sounding of the Lithosphere, *Geophys. J. Int.*, 1990, vol. 102, pp. 283–286.

Glaznev, V.N., *Kompleksnye geofizicheskie modeli litosfery Fennoskandii* (Complex Geophysical Models of Fennoscandia Lithosphere), Apatity: KaeM, 2003.

Ioffe, A. D., *Mekhanicheskie i elektricheskie svoistva kristallov* (Mechanical and Electric Properties of Crystals), Leningrad: Nauka, 1974.

Kaikkonen, P., Moisio, K., and Heeremans, M.,Thermomechanical Lithospheric Structure of the Central Fennoscandian Shield, *Phys. Earth Planet. Inter.*, 2000, no. 119, pp. 209–235.

Kononov, Yu.M. and Zhamaletdinov, A.A., Systems for ULF Radio Communication and Environmental Monitoring: A Challenging Trend in the Conversion Policy of Russia, *Radioelektronika i telekommunikatsii*, 2002, no. 2, pp. 4–6.

Korja, T., Engels, M., Zhamaletdinov, et al., Crustal Conductivity in Fennoscandia—a Compilation of a Database on Crustal Conductivity in Fennoscandian Shield, *Earth, Planets, Space*, 2002, no. 54, pp. 535—558.

Kovtun, A.A., Moiseev, O.N., Vagin, S.A., et al., MT and AMT soundings in Kola Peninsula and Karelia, in *Glubinnaya elektroprovodnost' Baltiiskogo shchita* (Deep Electric Conductivity of the Baltic Shield), Van'yan, L.L. and Kh'elt, S.E., Eds., Petrozavodsk: izd-vo Karel'sk. fil. AN SSSR, 1986.

Kraev, A.P., Semenov, A.S., and Tarkhov, A.G., Ultradeep Electric Sounding, *Razv. Nedr*, 1947, no. 3, pp. 40–41.

Maeda, K. and Matsumoto, H., Conductivity of the Ionosphere and Current System, *Rept. Ionosph. Space Res. Jap.*, 1962, no. 16, pp. 1–26.

Parkhomenko, E.I. and Bondarenko, A.T., *Elektroprovodnost' gornykh porod pri vysokikh davleniyakh i temperaturakh* (Electric Conductivity of Rocks under High Pressure and Temperature), Leningrad, 1972.

Pavlenkova, N.I., Structure of the Lithosphere within the Baltic Shield According to DSS Data, in *Struktura i dinamika litosfery Vostochnoi Evropy* (Structure and Dynamics of the East European Lithosphere), Moscow: Geokart, GEOS, 2006, pp. 33–58.

Paznukhov, V.E., Budanov, O.V., Rokhman, A.G., and Aristov, Yu.V., ELF Receiving Complex with VHF Retransmitter, *Radiofiz. Radioastron.*, 2010, vol. 15, no. 1, pp. 39–49.

Porokhova, L.N. and Kharlamov, M.M., The Solution of the One-Dimensional Inverse Problem for Induction Soundings by an Efficient Linearization Technique, *Phys. Earth Planet. Inter.*, 1990, vol.60, pp. 68—79.

Pozhilenko, V.I., Gavrilenko, B.V., Zhirov, D.V., and Zhabin, S.V., *Geologiya rudnykh raionov Murmanskoi oblasti* (Geology of the Ore Districts in the Murmansk Region), Apatity: MPR RF, 2002.

Rokityanskii, I.I., Zybkin, K.Yu., Rokityanskaya, D.A., and Shchepetnev, R.V., Magnetotelluric Studies of the Rock Massif at Borok, Lovozero and Petropavlovsk-Kamchatsky Geophysical Stations, *Elektromagnitnye zondirovaniya i magnitotelluricheskie metody razvedki* (Electromagnetic Soundings and Magnetotelluric Methods of Survey), Bryunelli, B.E., Ed., Leningrad: LGU, 1963, pp. 124–130.

Sapuzhak, Ya.S. and Enenshtein, B.S., The Use of the Electric Currents Generated by Power Transmission Lines in Electromagnetic Sounding of the Earth, *Dokl. Akad. Nauk,* 1980, vol. 252, no. 4, pp. 838–841.

Shevtsov, A.N., The Method of Frequency Sounding in the Study of Electric Conductivity in the Upper Crust of the Baltic Shield, *Extended Abstract of Cand. Sci. (Phys&Math.) Dissertation*, St. Petersburg: Izd. SpbGU, 2001.

Shevtsov, A.N., Forward and Inverse Problems of Frequency Electromagnetic Sounding with Industrial Power Transmission Lines, *Teoriya i metodika glubinnykh elektromagnitnykh zondirovanii na kristallicheskikh shchitakh* (Theory and Methods of Deep Electromagnetic Sounding on Crystalline Shields), Apatity: KNTs RAN, 2006, pp. 171–181.

Spice, B.R., Depth of Investigation in Electromagnetic Sounding Methods, *Geophys.,* 1989, vol. 54, no. 7, pp. 872–888.

Tereshchenko, E.D., Grigor'ev, V.F., Barannik M.B., et al., A Set–Up Converter and Energy Transfer System of the "Energy-2" Generator for Electromagnetic Sounding and Monitoring of Zones of Earthquake Sources, *Seism.Prib.*, 2009, vol. 44, no. 4, pp. 43–65 [*Seismic Instruments* (Engl. Transl.), 2009, vol. 45, no. 1, pp. 119–133].

Tikhonov, A.N., Enenshtein, B.S., and Skugarevskaya, O.A., The Study of the Inner Structure of the Crystalline Basement using Electromagnetic Sounding, *Dokl. Akad. Nauk SSSR*, 1967, vol. 173, no. 5, pp. 1062–1064.

Van Zijl, J.S.V., A Deep Slumberger Sounding to Investigate the Electrical Structure of the Crust and Upper Mantle in South Africa, *Geophys.*,1969, vol. 34, no. 3, pp. 450–462.

Vanyan, L.L., *Osnovy elektromagnitnykh zondirovanii* (Principles of Electromagnetic Sounding), Moscow: Nedra, 1965.

Vanyan, L.L., Berdichevskii, M.N., Vasin, N.D., et al., On a Normal Geoelectric Section, *Fiz.Zemli*, 1980, no. 2, pp. 73–76.

Varentsov, I.M., Engel's, M., Kor'ya, T., et al., A Generalized Geoelectric Model of Fennoscandia: A Challenging Database for Long-Period 3D Modeling Studies within the Baltic Electromagnetic Array Research (BEAR) Project, *Fiz. Zemli*, 2002, no. 10, pp. 64–105 [*Izv. Phys. Earth* (Engl. Transl.), 2002, vol. 38, no. 10, pp. 855–896].

Velikhov, E.P., Zhamaletdinov, A.A., Sobchakov, L.A., et al., On the Frequency Electromagnetic Sounding of the Earth's Crust using a Powerful ULF Antenna, *Dokl. Akad. Nauk SSSR*, 1994, vol. 338, no. 1, pp. 106–109.

Veshev, A.V., *Elektroprofilirovanie na postoyannom i peremennom toke* (Electric DC and AC Profiling), Leningrad: Nedra, 1980.

Zaborovskii, A.I., *Elektrorazvedka* (Electric Survey), Moscow: GNTINGTPL, 1963.

Zhamaletdinov, A.A., Kovalevskii, V.Ya., Pavlovskii, V.I., et al., Deep Electric Sounding with "Volgograd–Donbas" 800 kV DC PTL, *Dokl. Akad. Nauk SSSR*, 1982, vol. 265, no. 5, pp. 1101–1105.

Zhamaletdinov, A.A., *Model' elektroprovodnosti litosfery po rezul'tatam issledovanii s kontroliruemymi istochnikami polya (Baltiiskii shchit, Russkaya platforma)* (Electric Conductivity Model of the Lithosphere Based on the Results of Studies with Controlled Field Sources (Baltic Shield, Russian Platform)), Leningrad: Nauka, 1990.

Zhamaletdinov, A.A., Shevtsov, A.N., Tokarev, A.D., Kononov, Yu.M., and Van'yan, L.L., Influence of the Ionosphere and Bias Currents upon the Results of Deep Electromagnetic Soundings in the ELF Antenna Field, *Dokl. Akad. Nauk*, 1999, vol. 366, no. 5, pp. 688–691 [*Dokl. Earth Sci.* (Engl. Transl.), vol. 367, no. 5, pp. 678–681].

Zhamaletdinov, A.A., Korotkova, T.G., Tokarev, A.D., et al., Superdeep Sounding of the Lithosphere in the Baltic Shield Using Industrial Electric Power Lines, *Dokl. Akad. Nauk,* 2005, vol. 405, no. 5, pp. 666–669 [*Dokl. Earth Sci.* (Engl. Transl.), 2005, vol. 405, no. 9, pp. 1373–1376].

Zhamaletdinov, A.A., Shevtsov, A.N., Korotkova, T.G., et al., Deep Sounding with Industrial Power Lines in Conjunction with MTS Measurements, *Fiz. Zemli*, 2007, no. 3, pp. 74–80 [*Izv. Phys. Earth* (Engl. Transl.), 2007, vol. 43, no. 3, p. 259–265].

Zharkov, V.N., *Vnutrennee stroenie zemli i planet* (Inner Structure of the Earth and Planets), Moscow: Nauka, 1978.

Zhdanov, M.S., *Elektrorazvedka* (Electrical Survey), Moscow: Nedra, 1986.

Zonge, K.L. and Hughes, L.J., Controlled Source Audio–Frequency Magnetotellurics, *Electromagnetic Methods in Applied Geophysics—Theory and Practice*, M.N. Nabighian, Ed., Soc. Expl. Geophys., 1991, vol. 2B, pp. 713—809.